Test of Time-Reversal Invariance in the Reactions $^{16}O(d, \alpha)^{14}N$ and $^{14}N(\alpha, d)^{16}O$†

S. T. Thornton,* C. M. Jones, J. K. Bair, M. D. Mancusi,‡ and H. B. Willard§
Oak Ridge National Laboratory, Oak Ridge, Tennessee 37830
(Received 1 May 1970)

An experiment to study time-reversal invariance by both absolute and relative tests of detailed balance in the reaction $^{16}O(d, \alpha)^{14}N$ and its inverse has been performed. Measurements were made at three different excitation energies in a region where compound-nuclear resonances are resolved but overlapping levels are involved. In all cases the results are consistent with the principle of detailed balance, and our lowest uncertainty was ±0.5%. By making reasonable assumptions, an upper limit of 0.2% was assigned to the time-reversal-noninvariant part of the reaction amplitudes.

I. INTRODUCTION

The quest for broken symmetries has generated many new experiments in particle and nuclear physics. Tests of time-reversal invariance are particularly interesting because of the violation of CP symmetry in the decay of the K_2^0 meson observed in 1964 by Christenson, Cronin, Fitch, and Turlay.[1] CPT invariance links the observed CP violation with T violation. Although strong theoretical arguments can be made for assuming CPT invariance, the experimental uncertainty for CPT invariance in weak interactions is about the same order of magnitude as the observed CP violation. Therefore, direct experimental studies of time-reversal invariance are of great fundamental importance.

It is not possible to determine from the K_2^0 decay experiments alone whether the CP asymmetry is due to the weak, the electromagnetic, or the strong component of the interaction.[2] A new superweak interaction proposed by Wolfenstein[3] and by Lee and Wolfenstein[4] has been put in doubt, but not definitely excluded, by recent experiments.[5,6] Suggestions[4,7,8] have also been made that there might be a small C and/or T asymmetry in the strong interaction, or that the electromagnetic interaction strongly violates both C and T symmetry. The experimental sensitivity for detecting these asymmetries is expected to vary greatly depending upon the interaction responsible and the type of experiment.

We shall briefly review the experiments that specifically test time-reversal invariance. Such experiments began about the time that parity nonconservation was discovered.[9] Burgy *et al.*,[10] Clark and Robson,[11] and Erozolimsky *et al.*[12] have measured the electron-neutrino correlation from the β decay of polarized neutrons. Erozolimsky *et al.*[12] found that the phase angle between the vector and axial-vector amplitudes (which must be 0 or 180°, if the interaction is T invariant and if final-state interactions can be neglected) is $178.7 \pm 1.3°$. Similar measurements by Calaprice *et al.*[13] on the β decay of polarized ^{19}Ne nuclei give $180.2 \pm 1.6°$ for this phase angle. Thus, in these examples of leptonic weak interactions, time-reversal invariance holds to better than a few percent in amplitude.

Tests of T invariance in the electromagnetic interaction can be made by measuring the relative phase of multipole amplitudes of the nuclear matrix elements in mixed γ-ray transitions (again 0, or 180°, is expected under time-reversal invariance). Fuschini *et al.*[14] report $\sin\Phi = (3 \pm 4) \times 10^{-2}$ for the 1045-keV transition of ^{106}Rh. Kajfosz, Kopecký, and Honzátko[15] obtain the value $(-1.6 \pm 2.0) \times 10^{-2}$ for the 340-keV transition in ^{48}Ti. Employing the Mössbauer effect on the 90-keV transition in ^{99}Ru, Kistner[16] increased the sensitivity to find the result $\sin\Phi = (-1.0 \pm 1.7) \times 10^{-3}$. In a similar experiment with ^{193}Ir, Atac, Chrisman, Debrunner, and Frauenfelder[17] find $\sin\Phi = (1.1 \pm 3.8) \times 10^{-3}$. Zech, Wagner, Körner, and Kienle[18] obtain the limit 5×10^{-3} for ^{193}Ir. Perkins and Ritter[19] have observed a value of $(4 \pm 18) \times 10^{-3}$ for the decay of ^{106}Rh.

Nuclear reactions also furnish fruitful methods of testing time-reversal invariance, since this symmetry is a sufficient, *but not necessary*, condition for reciprocity. The unitarity of the scattering matrix alone often implies reciprocity. Moreover, as pointed out by Lee,[2] it is virtually impossible to experimentally produce the exact coherent time-reversed state for a particular reaction. Nonetheless, tests of reciprocity in nuclear reactions can be sensitive to small violations of T in the strong interaction and large violations of T in the electromagnetic interaction. Precision experiments in the range of 0.1 to 1% are therefore of considerable interest. However, the relationship between experimental results and upper limits for T-odd (noninvariant) terms in the interaction Hamiltonian is subject to theoretical interpretation

which is often model dependent and therefore subject to ambiguous interpretation.

The polarization-asymmetry equality follows directly from the necessary and sufficient condition of time-reversal invariance. Early experimental tests of this equality by Oxley *et al.*,[20] Hillman, Johansson, and Tibell,[21] Abashian and Hafner,[22] Rosen and Brolley,[23] and Hwang, Ophel, Thorndike, and Wilson[24] set limits of ±2 to ±6% for the polarization-asymmetry difference. McDonald, Haeberli, and Morrow[25] have obtained the more precise value of ±1.3% for p-^{3}He scattering at 10 MeV and 60° (c.m.), where the polarization is about 10%. Gross, Malanify, van de Woude, and Zucker[26] have set a limit of ±2.5% by scattering 33-MeV protons from ^{13}C at 60° (c.m.). A test of T invariance in p-p triple scattering at 430 MeV by Handler *et al.*[27] gives a polarization difference of $0.2 \pm 0.9\%$. This places an upper limit of 0.5% for the T-nonconserving amplitude.

Detailed-balance experiments have played an important role in time-reversal studies. Again, the early experiments by Rosen and Brolley,[23] (absolute data) and Bodansky *et al.*[28] (relative data) were of the order ±6% for the ratio of forward-to-inverse cross-section measurements. Precision relative cross-section measurements have been reported by Weitkamp *et al.*[29,30] for the ^{24}Mg(d,p)-^{25}Mg reaction and its inverse. This reaction, which is predominantly a direct process at their bombarding energies of 10 to 15 MeV, is found to satisfy detailed balance to about ±0.3%. Similarly, von Witsch, Richter, and von Bretano[31] have studied the ^{27}Al$(p, \alpha)^{24}$Mg reaction at bombarding energies of 10 to 15 MeV, where the reaction proceeds predominantly by compound-nucleus formation with a statistical fluctuation of the many overlapping energy levels. Their results agree with detailed balance to within ±0.6%.

Barshay[32] has pointed out that a violation of time-reversal invariance in the electromagnetic interaction may be observed by deviations from reciprocity by the reaction D$(\gamma, n)p$ and its inverse. Measurements have been made at photon energies from 240 to 320 MeV by Sober *et al.*[33] and Anderson, Prepost, and Wiik.[34] These are to be compared with neutron measurements at 600 MeV by Bartlett *et al.*[35] and Longo.[36] Although preliminary results showed deviations of at least 20% from detailed balance, it is now thought that instrumental errors are responsible. Thus, no violations of detailed balance have yet to be observed.

Some of the most fundamental tests of time-reversal symmetry are the studies of possible electric-dipole moments of elementary particles. Earlier measurements have recently undergone considerable refinement. Thus, upper limits of $|d/e| \leq 5 \times 10^{-23}$ cm for the dipole moment of the neutron have been set by Baird, Miller, Dress, and Ramsey.[37] Harrison, Sandars, and Wright[38] have found $|d/e| = (7 \pm 9) \times 10^{-21}$ cm for the proton. Weisskopf *et al.*[39] have obtained a value of $|d/e| < 3 \times 10^{-24}$ cm for the electron by a study of the cesium atom. A somewhat poorer value of $|d/e| \leq 2 \times 10^{-16}$ cm for the muon has been established by Berley and Gidal.[40] All measurements are consistent with time-reversal invariance and the limits in the range 10^{-22} to 10^{-24} cm are gradually eliminating many of the possible theoretical explanations for the observed violation of CP.

There have been a number of other experiments[41] in particle physics searching for deviations from T symmetry. Subject to the ambiguities of interpretation, no experimental violation has yet been observed.

Our experiment has been reported in summary[42] form. It was designed to detect a possible noninvariance of time reversal by precision measurements of detailed balance in a nuclear reaction which proceeds through a compound-nucleus reaction in an excitation region where the energy levels are still somewhat resolved but overlapping. A study indicated that the reaction ^{16}O$(d, \alpha)^{14}$N and its inverse was a good choice. The following section is devoted to theoretical and experimental considerations of the problem. In Sec. III we discuss the apparatus and in Sec. IV the experimental procedure is described. Corrections and uncertainties for these data are discussed separately in Sec. V. The final experimental results are presented in Sec. VI, and the detailed-balance comparisons are presented in Sec. VII. The interpretation and conclusions are discussed in the final section.

II. THEORETICAL AND EXPERIMENTAL CONSIDERATIONS

The principle of detailed balance (or more precisely "semidetailed" balance as used in the present context[43]) relates the differential cross sections for a reaction, $a + A \rightarrow b + B$, and its inverse. If $\sigma'(\theta)$ represents the c.m. differential cross section for unpolarized beams and targets at a c.m. scattering angle θ, then detailed balance can be represented by the equality

$$\frac{\sigma'_{b\rightarrow a}(\theta)}{\sigma'_{a\rightarrow b}(\theta)} \frac{P_b^{\,2}}{P_a^{\,2}} \frac{(2S_b+1)(2S_B+1)}{(2S_a+1)(2S_A+1)} = 1, \tag{1}$$

where P is the c.m. momentum of the projectile particle, and S is the intrinsic particle spin. The inverse differential cross sections must be compared at the same c.m. angle and excitation energy.

A difficult task in testing T by detailed balance

is choosing a reaction that is both sensitive to a violation of T and experimentally practical. Several theoretical papers have been published concerning the sensitivity of detailed balance to T violation.[44-52] Criteria suggested in these theoretical works were followed in choosing our reaction.

The first criteria for a detailed balance reaction were presented several years ago by Henley and Jacobsohn.[44] They suggested that one should choose a reaction with a complicated reaction mechanism and with many competing open channels. In some special cases they concluded that the unitarity of the scattering matrix alone implies detailed balance. Time-reversal invariance implies detailed balance, but detailed balance does not necessarily imply T symmetry.

There has recently been much discussion concerning the sensitivity of detailed balance to T violation in direct reactions and in compound statistical or "Ericson" fluctuating reactions. Several authors[49,50,52] have indicated that direct reactions may not be suitable for investigating T violation by the detailed-balance method, although numerical calculations by Henley and Huffman indicate that this may not be true.[51] Mahaux and Weidenmüller[46] showed that a single-level-resonance compound-nucleus reaction is not suitable for T investigation, since detailed balance always holds in that case. They indicated that the two-overlapping-level-resonance case might be a good situation to investigate. Krieger[47] concluded that detailed balance is obeyed on the average, even if T is violated, in the region of many strongly overlapping resonances or "Ericson" fluctuations. On the other hand, Ericson,[45] Mahaux and Weidenmüller,[46] and Moldauer[50,52] concluded that the region of statistical fluctuations would be a good region in which to detect T violation.

Ericson[45] has also pointed out that one should choose a reaction in which a single amplitude dominates. Then detailed balance will most closely resemble the reciprocity relation. If there are many interfering amplitudes, then the sensitivity for observing a T-violation effect may be substantially reduced.

Experimental criteria are dictated by a number of factors. Absolute differential cross-section measurements might be expected to have greater sensitivity to T violation than relative data. In the latter case the effect must be a function of either energy or angle in order to be detected. High-precision absolute cross sections require stable gaseous targets of high isotopic and chemical purity. The ground states of the residual nuclei should be easily resolved experimentally from their first excited states. A low Q value is helpful in performing both the forward and inverse reactions under similar conditions.

The above criteria were used in selecting the reaction $^{16}O(d, \alpha)^{14}N$ and its inverse to study. It is interesting to note that the same reaction was independently chosen at the University of Wisconsin.[53] The experiment at Wisconsin was originally studied near the same energy and angle as the present experiment.

At the bombarding energies available with the Oak Ridge National Laboratory (ORNL) 6-MV and tandem Van de Graaff accelerators, there are a large number of open channels in the $^{16}O(d, \alpha)^{14}N$ reaction. At about 11.4-MeV excitation the reaction proceeds primarily by compound-nucleus formation, rather than by direct reaction. This region of the compound nucleus is one of a few interfering levels.

There are nine reaction amplitudes possible for this reaction, only five of which are independent under the assumption of parity conservation. Furthermore, three of these five contain angular factors which approach zero at least as fast as $\sin\theta$ as the scattering angle θ approaches 0 or 180°. In order to minimize any possible destructive-interference effects of these three amplitudes, our measurements were made at the most backward angle experimentally available, approximately 162.2° in the c.m. system.

Both targets for this experiment are gases which can be obtained with high isotopic and chemical purity.

III. APPARATUS

In this section we will describe briefly the experimental apparatus. A more complete discussion of those aspects most relevant to our measurements will be given in Sec. V. A complete description of the gaseous-target scattering chamber used for the experiment has been published.[54]

The scattering chamber was operated in the differential pumping mode[54] with a 0.000 25-cm Havar[55] foil separating the target gas from the Faraday-cup vacuum system. All of the detailed-balance cross-section data were measured with the 0.317 × 1.587-cm movable-slit system.[54] Since the same detector slit system was used for both forward and inverse cross-section measurements, uncertainties in the slit-system dimensions cancel out in the detailed-balance comparisons. Also the same detector (Nuclear Diodes, Inc., serial No. 950) was used throughout the experiment. Its properties have been described in detail.[56] For monitoring purposes, data were also recorded for detectors located at other fixed angles. Spectra for the movable and fixed detectors were recorded

in 512-channel groups of a multichannel analyzer which was gated by single-channel analyzers. Pulses from the single-channel analyzers were also counted in 10- and 100-MHz scalers.

α-particle beams required for the experiment were produced by accelerating doubly-charged helium ions in the ORNL 6-MV Van de Graaff accelerator. This accelerator also generated deuteron beams for the preliminary measurements. However, the final $^{16}O(d, \alpha)^{14}N$ cross sections obtained for the precision detailed-balance comparisons were measured with the ORNL tandem accelerator (because of scheduling considerations).

IV. PROCEDURE

Excitation functions for the $^{16}O(d, \alpha)^{14}N$ reaction in the deuteron bombarding energy range 3.6 to 5.3 MeV and for the $^{14}N(\alpha, d)^{16}O$ reaction in the α-particle bombarding energy range 8.5 to 10.0 MeV were measured at several angles in order to locate optimum conditions for performing the tests of detailed balance. We particularly sought an energy region which included a sharp resonance (peak) to serve as a precise energy intercalibration for the forward and inverse reactions. An energy region in which the cross section would not vary appreciably with bombarding particle energy was also desired.

Satisfactory energy regions were found in the $^{16}O(d, \alpha)^{14}N$ reaction in the deuteron bombarding energy range 4.3 to 4.8 MeV at a laboratory angle of 160° as shown in Fig. 1. Precision cross sections were measured at three energies and $\theta_{lab} = 160°$ for the $^{16}O(d, \alpha)^{14}N$ reaction: (1) 4.40 MeV (peak), (2) 4.58 MeV (valley), and (3) 4.71 MeV (plateau). Measurements were made at the corresponding inverse energies and angles for the $^{14}N(\alpha, d)^{16}O$ reaction. Angular distributions for the $^{16}O(d, \alpha)^{14}N$ reaction measured for laboratory scattering angles of 20 to 160° over the peak, valley, and plateau are shown in Figs. 2–4.

In the $^{16}O(d, \alpha)^{14}N$ reaction, differential cross sections were measured over the peak, valley, and plateau regions with small energy steps and several target-gas pressures. In the peak region, measurements were made in 2.5-keV steps at pressures of 0.007, 0.015, and 0.024 atm. In the valley region, measurements were made in 2.5-keV steps at pressures of 0.007 and 0.024 atm. Measurements in the plateau region were made in 5-keV steps at pressures of 0.007 and 0.024 atm.

In the $^{14}N(\alpha, d)^{16}O$ reaction, measurements were made at only one energy each for the peak, valley, and plateau. The proper laboratory scattering angle for detailed-balance comparisons changed slightly with energy, but was about 157°. Counting rates were much lower than in the $^{16}O(d, \alpha)^{14}N$ reaction and a number of runs at each energy were made to collect a statistically significant number of counts. The target-gas pressure was about 0.008 atm for the peak and valley and about 0.016 atm for the plateau.

While recording the precision data, the current integrator was calibrated about every 2 h. The chamber gas pressure and temperatures were measured about every 25 min. Dead times in the analyzer were typically 2% while recording the $^{16}O(d, \alpha)^{14}N$ data, and 1% while recording the $^{14}N(\alpha, d)^{16}O$ data.

In addition to the detailed-balance data several other measurements were made. The 90° analyzing magnet was calibrated and the energy loss of the beam particles traveling through the gas was measured in order to determine the target energy of the bombarding particles. Several experiments pertaining to data corrections were performed. These measurements included slit-edge scattering, detector inefficiency, gas heating by the beam, detector-spectrum shape, and ^{17}O, ^{18}O,

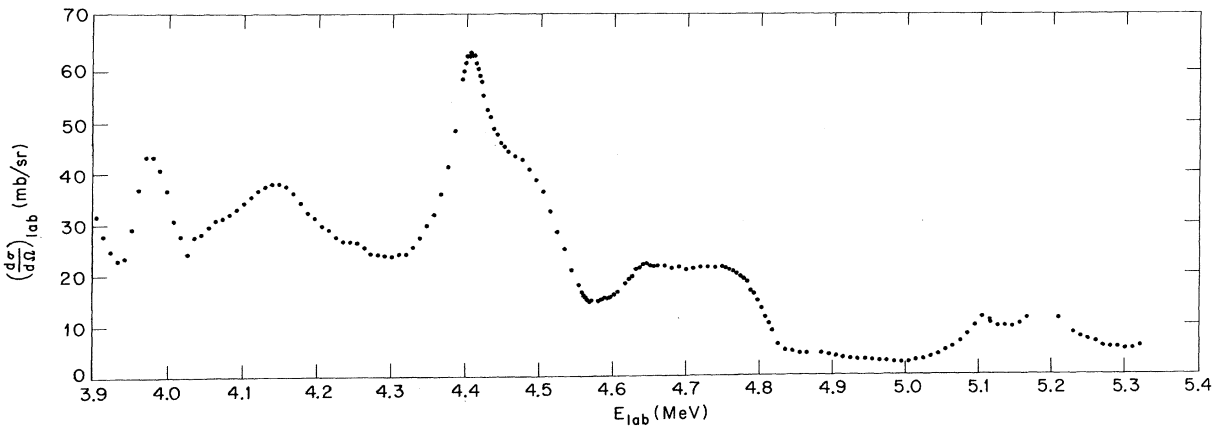

FIG. 1. Laboratory excitation function for the $^{16}O(d, \alpha)^{14}N$ reaction at $\theta_{lab} = 160°$.

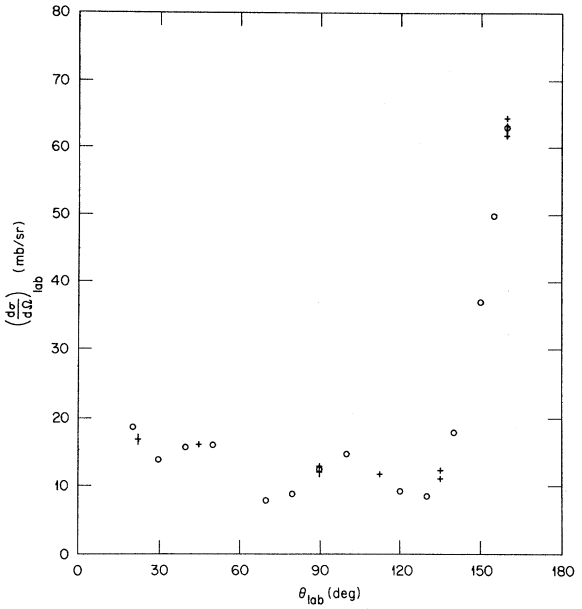

FIG. 2. Laboratory angular distribution for the $^{16}O(d, \alpha)^{14}N$ reaction at E_{lab} (deuteron) = 4.405 MeV (peak). The different data symbols indicate measurements made at various times.

and ^{15}N isotopic corrections. These measurements are discussed separately in the next section.

V. CORRECTIONS AND UNCERTAINTIES

Several of the corrections that were considered in the present experiment have been discussed elsewhere.[56] Each correction, either measured or calculated, was assumed to be the mean value of a normal distribution. All uncertainties quoted are standard deviations. Corrections $\leq 0.01\%$ were generally neglected and uncertainties $\leq 0.03\%$ were considered negligible. Typical corrections and uncertainties for the various effects are given in Tables I and II for the reactions $^{16}O(d, \alpha)^{14}N$ and $^{14}N(\alpha, d)^{16}O$, respectively.

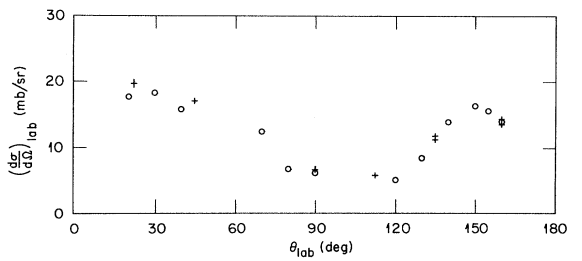

FIG. 3. Laboratory angular distribution for the $^{16}O(d, \alpha)^{14}N$ reaction at E_{lab} (deuteron) = 4.578 MeV (valley). The different data symbols indicate measurements made at various times.

A. Number of Incident Beam Particles

1. Current Integration

The number of incident beam particles was determined by measuring the integrated beam current through the Faraday cup by means of a current integrator. The leakage of the current integrator was measured with no beam and was found to be negligible. There was a small dependence of the current-integrator calibration associated with the room temperature. The uncertainty in the current-integrator calibration was estimated to be $\pm 0.13\%$ in the $^{14}N(\alpha, d)^{16}O$ reaction and $\pm 0.05\%$ in the $^{16}O(d, \alpha)^{14}N$ reaction.

2. Faraday Cup

Two main problems were associated with the Faraday cup: suppression of secondary electrons and ionization of the residual gas by the beam.[54]

The beam passing through the foil separating the high-vacuum Faraday-cup region from the chamber produced secondary electrons. Later when the beam struck the rear of the Faraday cup additional secondary electrons were produced. A net transfer of electrons, either to or from the Faraday cup, resulted in an error in the current integration. Therefore, a suppressor electrode maintained at a potential of -1000 V was located between the foil and the Faraday cup to prevent a net transfer of electrons to or from the Faraday cup.

A test of the effectiveness of the suppression voltage was performed by varying the voltage and comparing it with the number of current-integrator counts normalized to the number of reaction counts in a detector in the chamber. At low suppression voltages the number of normalized current-integrator counts was high indicating that electrons were leaving the Faraday cup and, in effect, causing a more positive charge to be measured. From -300 to -1500 V, however, the number of normalized current-integrator counts was

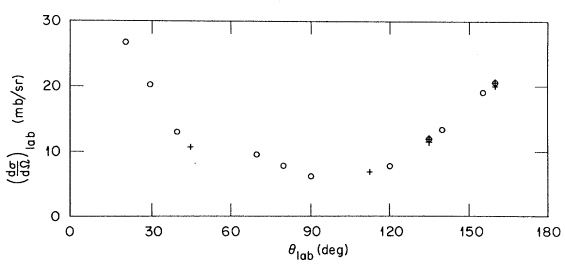

FIG. 4. Laboratory angular distribution for the $^{16}O(d, \alpha)^{14}N$ reaction at E_{lab} (deuteron) = 4.710 MeV (plateau). The different data symbols indicate measurements made at various times.

TABLE I. Typical data correction factors ± uncertainties for the $^{16}O(d,\alpha)^{14}N$ reaction. Correction (in percent) ± uncertainty (in percent) to $(d\sigma/d\Omega)_{lab}$.

Effect	Peak 0.008 atm	Peak 0.024 atm	Valley 0.008 atm	Valley 0.024 atm	Plateau 0.008 atm	Plateau 0.024 atm
Faraday-cup ionization	−0.01 ± 0.01	−0.01 ± 0.01	−0.01 ± 0.01	−0.01 ± 0.01	−0.01 ± 0.01	−0.01 ± 0.01
Compensation	0.02 ± 0.05	0.06 ± 0.10	0.02 ± 0.05	0.06 ± 0.10	0.02 ± 0.05	0.06 ± 0.10
Beam-aperture scattering	0.05 ± 0.05	0.05 ± 0.05	0.05 ± 0.05	0.05 ± 0.05	0.05 ± 0.05	0.05 ± 0.05
Beam-current dependence	0.15 ± 0.16	0.50 ± 0.06	0.15 ± 0.16	0.50 ± 0.06	0.15 ± 0.16	0.50 ± 0.06
Beam-scattering loss	−0.35 ± 0.05	−0.38 ± 0.05	−0.32 ± 0.05	−0.35 ± 0.05	−0.31 ± 0.05	−0.34 ± 0.05
Natural gas	0.24 ± 0.	0.24 ± 0.	0.24 ± 0.	0.24 ± 0.	0.24 ± 0.	0.24 ± 0.
Slit-edge scattering	0. ± 0.04	0. ± 0.04	0. ± 0.04	0. ± 0.04	0. ± 0.04	0. ± 0.04
Detector inefficiency	0.11 ± 0.05	0.11 ± 0.05	0.11 ± 0.05	0.11 ± 0.05	0.11 ± 0.05	0.11 ± 0.05
Typical analyzer dead time	2.1 ± 0.05	4.0 ± 0.10	1.3 ± 0.05	2.0 ± 0.05	1.2 ± 0.05	1.9 ± 0.05
Unideal gas	0.01 ± 0.	0.02 ± 0.	0.01 ± 0.	0.02 ± 0.	0.01 ± 0.	0.02 ± 0.
^{17}O and ^{18}O peaks	0. ± 0.03	0. ± 0.06	−0.03 ± 0.03	−0.03 ± 0.06	−0.01 ± 0.03	−0.01 ± 0.06
Spectrum background	−0.23 ± 0.04	−0.22 ± 0.04	−0.62 ± 0.08	−0.62 ± 0.11	−0.47 ± 0.07	−0.55 ± 0.09
Current integration	0. ± 0.05	0. ± 0.05	0. ± 0.05	0. ± 0.05	0. ± 0.05	0. ± 0.05
Secondary-electron suppression	0. ± 0.05	0. ± 0.05	0. ± 0.05	0. ± 0.05	0. ± 0.05	0. ± 0.05
Pressure reading	0.01 ± 0.17	0.04 ± 0.12	−0.01 ± 0.17	0.08 ± 0.12	0.01 ± 0.17	+0.11 ± 0.12
Manometer oil density	0. ± 0.04	0. ± 0.04	0. ± 0.04	0. ± 0.04	0. ± 0.04	0. ± 0.04

statistically constant. No loss due to secondary electrons was assumed and an uncertainty of ±0.05% was assigned to the current integration at a suppression voltage of −1000 V.

If a beam particle ionizes a gas particle in the Faraday cup, a spurious result may occur in the current integration due to the presence of the high suppression voltage. For this reason a high vacuum was needed in the Faraday-cup region. An estimate of the error due to this ionization was made for the α beam particles by measuring the current through the suppressor electrode as a function of the pressure in the Faraday cup. The correction made to the beam-current integration was +0.025% per 10^{-6} Torr pressure in the Faraday cup for the α beam and was calculated to be +0.006% per 10^{-6} Torr pressure for the deuteron beam. The pressure in the Faraday cup varied from (1 to 3) × 10^{-6} Torr during the experiment. The uncertainty assigned to this correction was equal to the correction applied.

3. *Beam Impurities*

In order to search for beam impurities, the reaction-product spectra were examined for reactions that impurities may produce. There were

TABLE II. Typical data correction factors ± uncertainties for the $^{14}N(\alpha,d)^{16}O$ reaction. Correction (in percent) ± uncertainty (in percent) to $(d\sigma/d\Omega)_{lab}$.

Effect	Peak 0.008 atm	Valley 0.008 atm	Plateau 0.016 atm
Faraday-cup ionization	−0.05 ± 0.05	−0.05 ± 0.05	−0.05 ± 0.05
Charge state of beam particle	−0.23 ± 0.02	−0.23 ± 0.02	−0.23 ± 0.02
Beam-aperture scattering	0.14 ± 0.07	0.14 ± 0.07	0.14 ± 0.07
Beam-current dependence	0.06 ± 0.02	0.05 ± 0.02	0.06 ± 0.02
Pressure reading	0.18 ± 0.23	0.18 ± 0.23	0.09 ± 0.13
^{15}N peaks	−0.01 ± 0.01	−0.30 ± 0.05	−0.05 ± 0.02
Natural gas	0.36 ± 0.	0.36 ± 0.	0.36 ± 0.
Slit-edge scattering	−0.07 ± 0.11	−0.07 ± 0.11	−0.07 ± 0.11
Detector inefficiency	0.02 ± 0.05	0.02 ± 0.05	0.02 ± 0.05
Typical analyzer dead time	1.0 ± 0.05	1.0 ± 0.05	1.0 ± 0.05
Beam-scattering loss	−0.34 ± 0.06	−0.33 ± 0.06	−0.33 ± 0.06
Spectrum background	−0.37 ± 0.08	−2.13 ± 0.15	−2.45 ± 0.15
Unideal gas	0.01 ± 0.	0.01 ± 0.	0.02 ± 0.
Compensation	0.02 ± 0.05	0.02 ± 0.05	0.04 ± 0.08
Current integration	0. ± 0.13	0. ± 0.13	0. ± 0.13
Secondary-electron suppression	0. ± 0.05	0. ± 0.05	0. ± 0.05
Beam impurities	0. ± 0.05	0. ± 0.05	0. ± 0.05
Manometer oil density	0. ± 0.04	0. ± 0.04	0. ± 0.04

no detectable reactions due to impurities in either the deuteron or α beam. A negligible uncertainty was assigned for the deuteron beam and an uncertainty of ±0.05% was assigned for the α beam.

4. *Charge State of the α-Particle Beam*

When the α beam particles passed through the Havar foil into the Faraday cup, a small fraction of the α particles emerged as singly charged. The resultant effective charge of the α particles must be known in order to determine the number of incident beam particles from the current integration. The effective charge of the α particles at 8.2 MeV was taken to be $+1.9954e$ from the work of Allison.[57] An uncertainty of ±0.02% was assigned to this value for the present experimental conditions.

5. *Scattering Loss of Beam*

The number of incident beam particles passing through the gaseous target volume must be known in order to calculate the absolute differential cross section. Since the beam charge was actually measured in the Faraday cup, the possibility of a loss of beam particles between the target volume and Faraday cup was examined. The loss of beam due to scattering by the gas between the target volume and the Havar foil was calculated to be negligible. The loss of beam by multiple scattering in the Havar foil was also calculated to be negligible, but the loss due to single Rutherford scattering in the foil was not negligible. This loss varied with the pressure and beam energy and was calculated to be about −0.35% for the deuteron beam and about −0.34% for the α beam for measurements at the peak. Uncertainties of ±0.05% and ±0.06% were assigned to this correction for the deuteron and α beams, respectively.

6. *Beam-Aperture Scattering*

The beam-defining and differential-pumping apertures in front of the scattering chamber were designed so that a minimal number of beam particles scattered from these apertures would reach the target volume.[54] Beam particles scattered from apertures have lower energies and should be excluded from the cross-section measurement. In an associated experiment,[56] a determination was made of the energy degradation of the beam due to aperture scattering. A correction for this effect was made in the differential cross-section measurements by excluding such particles in determining the total number of counts in the peak and by a corresponding correction to the current-integration result. The correction to the current integration was $(-0.14 \pm 0.07)\%$ for the α beam and $(-0.05 \pm 0.05)\%$ for the deuteron beam.

B. Target Nuclei Density

The number of target nuclei per unit volume, N, was determined to first order by measuring the pressure and temperature of the gas. In an ideal gas these are related by the equation,

$$N = 2L_0(P/P_0)(T_0/T), \tag{2}$$

where L_0 is Loschmidt's number, the number of molecules per unit volume for an ideal gas at temperature T_0 (0°C) and pressure P_0 (760-mm Hg). P and T are the pressure and temperature, respectively, of the gas in the chamber. The factor 2 arises from the diatomic gases O_2 and N_2 used in this experiment. Corrections to the above equation are discussed below.

1. *Temperature Measurement*

The temperature of the gas was measured near the chamber wall, but this was not the temperature of the gas in the target volume because of local heating of the gas by the beam. Heat is carried away from the target by both conduction and convection. Since the flow pattern of the gas is unknown inside the chamber, the convection heat loss is very difficult to calculate. Since the beam-heating temperature effect could not be calculated, the effect was measured experimentally.

The beam-heating effect was determined by measuring the reaction-product yield as a function of beam current. As the beam current is increased, the target gas is heated, and the yield is decreased. If there are electronic losses due to high counting rates, the yield will be affected by the beam current in a similar manner. Therefore, the correction measured is really a beam-current-dependent correction. Considerable effort was made to keep the beam current from fluctuating, even over very short periods, so that the beam-heating and electronic effects would remain constant.

The dependence of the yield on beam current was measured in different ways for the $^{16}O(d, \alpha)^{14}N$ and $^{14}N(\alpha, d)^{16}O$ data. The current dependence of the yield was a relatively large effect, especially for the μA deuteron beams. For the $^{16}O(d, \alpha)^{14}N$ data, the dependence of the yield on beam current was measured directly by measuring the yield as a function of beam current. A linear least-mean-squares fit was made to these data and the yield intercept at zero beam current was taken as the true yield. This measurement was made at several energies and all pressures used for the $^{16}O(d, \alpha)^{14}N$ measurement. The over-all beam-current-de-

pendent effect for the $^{16}O(d, \alpha)^{14}N$ reaction is listed in Table I.

In order to separate the relative magnitudes of the beam-heating and electronic effects in the $^{16}O(d, \alpha)^{14}N$ data the following experiment was performed. At a given pressure the yield versus beam current was measured for several electronic counting rates by varying the scattering angle. Since the beam heating, but not the electronic loss, was constant at each angle, the electronic loss could be determined from the change with angle of the over-all beam current dependence.

In the $^{14}N(\alpha, d)^{16}O$ case we could not make a direct measurement of the beam-current dependence of the yield due to the small available beam current. In this case a singly-charged helium beam was used at an energy of ~5 MeV. The yield versus beam current was again measured and the dependence was then obtained from the slope. This result was extrapolated to ~9 MeV by the use of energy-loss curves[58] under the assumption that the beam-heating dependence is directly proportional to the ionization energy loss of the beam traveling through the gas. This effect was measured for both pressures employed in the $^{14}N(\alpha, d)^{16}O$ cross-section measurements.

The total beam-current-dependence correction for the $^{14}N(\alpha, d)^{16}O$ reaction was determined from the sum of the beam-heating and electronic-count-rate effects. The electronic-effect correction was that determined from the $^{16}O(d, \alpha)^{14}N$ data. The total correction to the cross section was determined to be typically $(0.06 \pm 0.02)\%$ for the $^{14}N(\alpha, d)^{16}O$ reaction.

2. Pressure Measurement

The chamber gas pressure was determined by reading the differences in height of the oil columns in a U-shaped manometer. The pressure is related to the difference in height H by

$$P = \rho g H, \tag{3}$$

where ρ is the density of the manometer oil and g is the local acceleration of gravity.

A correction, which should be zero for perfect alignment of the cathetometer, was made to H arising from the column-level difference measured at zero pressure. The zero correction was never more than 0.025 cm, and the total uncertainty assigned to the measurement of H varied between 0.12 and 0.23%. This uncertainty resulted from uncertainties in reading each individual measurement of H and the zero-level reading.

The manometer oil density was measured as a function of temperature by the ORNL Analytical Chemistry Division and the result compared favorably with that reported by Thomas and Cross.[59] There is a small temperature dependence of the oil density, so a thermometer was placed between the manometer tubes to indicate the oil temperature. The difference between the measured temperature and the actual oil temperature introduced a small uncertainty in the oil density. The density of the Dow Corning 704 manometer oil, ρ, was taken to be

$$\rho = 1.0615[1 + 68 \times 10^{-5}(25 - T)] \text{ g/cm}^3, \tag{4}$$

where T is the temperature (°C) measured at the manometer. The uncertainty in ρ was estimated to be ±0.04%.

The local acceleration of gravity g was taken[60] to be

$$g = 979.74 \text{ cm/sec}^2 \tag{5}$$

with an uncertainty which was considered to be negligible.

3. Imperfect-Gas Correction

Since relatively low pressures were used for the measurements, the ideal-gas assumption is a good one. Calculations showed that the correction ΔL to be made to Loschmidt's number for oxygen and nitrogen gases was (per atmosphere of chamber pressure) $\Delta L = -1\%/\text{atm}$.

4. Gas Impurities

Ultra-high-purity nitrogen and oxygen gases were used in order to eliminate gas impurities. The reaction spectra were closely examined for peaks due to impurity-gas reactions, but none were found. It was concluded that no measurable chemical impurities existed and the uncertainty due to gas impurities was negligible.

C. Energy

1. Beam-Energy Calibration and Resolution

The energy of the deuteron beam used for the final $^{16}O(d, \alpha)^{14}N$ measurements was defined by the 90° analyzing magnet of the tandem accelerator which was calibrated by the $^{27}Al(p, n)^{27}Si$ threshold reaction.[61] These measurements resulted in an absolute uncertainty of the mean deuteron beam energy of ±0.13%.

The peak at a deuteron bombarding energy of 4.40 MeV and angle of 160° in the $^{16}O(d, \alpha)^{14}N$ reaction served as an energy reference in the inverse reaction. Good agreement was obtained for the energy determination of the peak between the final measurements on the tandem accelerator and a preliminary measurement on the 5.5-MV accelerator. Since the energy of the inverse-reaction α-particle beam may be calculated from the Q val-

ue of the reaction, the absolute energy of the α beam was not required for detailed-balance comparisons. However, the $^{24}Mg(\alpha,\gamma)^{28}Si$ resonance at 3.1998 MeV[62] was measured as a calibration check. The Q value of the $^{16}O(d,\alpha)^{14}N$ reaction was taken to be 3.110 22 ± 0.000 38 MeV from *Nuclear Data Tables*.[63]

The resolution of the beam particle energy was primarily determined by the control slits located after the 90° analyzing magnet. The resolution was estimated to be ±0.04% for deuterons and ±0.05% for the α beam. The distribution of energies about the mean value was assumed to approximate a normal distribution, so that the quoted resolutions represent standard deviations.

2. *Beam-Energy Loss in Gas*

In order to determine the incident particle energy at the center of the gas target, the ionization energy loss of the beam particles traveling through the gas was experimentally measured. This was accomplished for both the deuteron and α beams by placing a solid-state detector in the middle of the chamber. Spectra were measured for very low beam currents at several different pressures at one beam energy. The shifts of the energy peak in the spectra indicated the beam-energy loss. Energy losses at other beam energies were obtained by extrapolation from standard energy-loss curves. Typical energy losses at a target pressure of 0.008 atm were 29 keV for the deuteron beam and 115 keV for the α-particle beam. The uncertainty in this energy loss was estimated to be ±10%.

The total uncertainty of the deuteron beam energy was due to the combined uncertainties in the beam energy and energy loss in the gas, and a typical value at 0.008 atm was ±6.7 keV.

3. *Straggling*

In order to compare the inverse cross sections the energy distribution of the beam particles in the target region must be known. The straggling of the beam particles through the gas was calculated by means of the simple Gaussian theory and Symon's more exact theory.[64] Typical standard deviations of the straggling energy spread due to the beam particles traveling to the target region at 0.008-atm gas pressure were ±4.1 keV for deuterons and ±8.6 keV for α particles.

4. *Target-Region Energy Thickness*

Particles entering the detector are scattered from a finite region of target gas along which the beam particles are losing energy. This target region is shown in Fig. 5 as a plane view of the beam and slit-system region. The actual intensity distribution of particles entering the detector slit system from the target region has a trapezoidal shape. Thus, the energy distribution due to the energy loss along the target region will be the same as the intensity distribution. Energy losses were calculated from the energy-loss curves of Whaling[58] and are given in Tables III and IV.

The total range of beam energy across the target region is determined by the beam-energy resolution, straggling of beam particles through the chamber gas, and ionization energy losses of the beam particles traveling through the target region. The beam-energy resolution, straggling, and target energy loss were convolved to determine the total target thickness. Typical total target thicknesses (standard deviations) at 0.008-atm pressure were ±5 keV for the $^{16}O(d,\alpha)^{14}N$ reaction and ±10 keV for the $^{14}N(\alpha,d)^{16}O$ reaction.

D. Number of Scattered Particles

1. *Scattering Compensation Processes*

As the scattered reaction products travel from the target volume through the gas toward the detector, as much as 5% of the particles that were originally going toward the detector may be scattered by the gas particles and miss the detector. Fortunately, there are processes which compen-

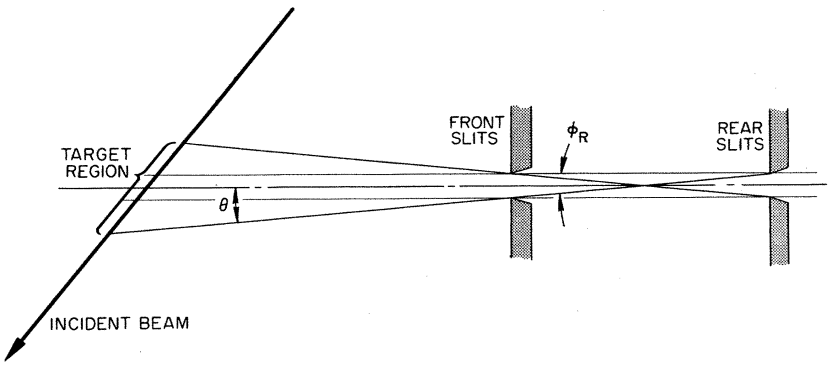

FIG. 5. Horizontal section of beam and slit-system region.

TABLE III. Experimental parameters for $^{14}N(\alpha,d)^{16}O$ cross sections.

Quantity	Peak	Valley	Plateau
Approximate laboratory bombarding energy (MeV)	9.03	9.23	9.38
Corresponding bombarding energy in the $d+^{16}O$ system [a] (MeV)	4.405 ± 0.002	4.578 ± 0.003	4.710 ± 0.007
Laboratory scattering angle [b]	157°6.5′ ± 1.0′	157°11.5′ ± 1.0′	157°15.5′ ± 1.0′
Laboratory cross section (mb/sr)	15.882	3.7382	5.5126
Statistical uncertainty in cross section	±0.33%	±0.41%	± 0.28%
Systematic uncertainty in cross section	±0.32%	±0.35%	± 0.30%
Target-gas pressure (atm)	0.008	0.008	0.016
Energy dispersion of beam entering scattering chamber (keV) [c]	5.1 ± 2.5	5.1 ± 2.5	5.3 ± 2.6
Width of straggling distribution (keV) [c]	8.6 ± 0.4	8.6 ± 0.4	12.1 ± 0.6
Target thickness (FWHM in keV)	7.2 ± 0.2	7.2 ± 0.2	14.7 ± 0.4

[a] The quoted uncertainty is relative to the energy scale established for the $^{16}O(d,\alpha)^{14}N$ reaction.
[b] The quoted uncertainty is the uncertainty relative to the angle setting for the inverse reaction.
[c] We assume the energy dispersion and straggling to be normal distributions. Quoted values for the widths are the standard deviations of those distributions. Uncertainties quoted are the uncertainties in the standard deviations. These uncertainty distributions are also assumed to be normal distributions.

sate for this scattering loss. These compensation processes have to be studied in great detail in order to make corrections when the compensation processes do not cancel.

The compensation processes and their effectiveness have been discussed in detail by Worthington.[65] His analysis has been followed in the evaluation of error corrections and uncertainties resulting from the compensation processes. These calculations showed that the corrections for the present experiment were very small. The uncertainty assigned to these calculations was typically ±0.05%.

2. *Slit-Edge Scattering*

The gaseous target region was defined by the slit edges of the front and rear slits. Ideally, particles hitting the slit edges should be completely stopped. In practice, however, particles hitting the slit edges can be scattered into the detector causing spurious counts in the energy spectrum. Particles which lose only a small amount of energy in the slit edge can produce counts near the spectral peak.

Slit-edge scattering was investigated in some detail for the present experiment.[56] These measurements indicated that the slit-edge scattering correction for $^{14}N(\alpha,d)^{16}O$ was $(-0.07\pm0.11)\%$ and for $^{16}O(d,\alpha)^{14}N$ was $0\pm0.04\%$.

3. *Detector Efficiency*

Solid-state-detector efficiencies may not be exactly 100%. Therefore, the efficiency of the surface-barrier detector was measured for both α particles and deuterons. Measurements were performed by scattering α particles from a deuterated polyethylene (CD_2) foil.[56] The efficiency *loss*

TABLE IV. Experimental parameters for $^{16}O(d,\alpha)^{14}N$ cross sections.

Quantity	Peak		Valley		Plateau	
	0.008 atm	0.024 atm	0.008 atm	0.024 atm	0.008 atm	0.024 atm
Approximate laboratory bombarding energy (MeV)	4.40	4.40	4.58	4.58	4.71	4.71
Systematic uncertainty in cross section [a]	±0.28%	±0.24%	±0.28%	±0.25%	±0.28%	±0.24%
Energy dispersion of beam entering scattering chamber (keV) [b]	2.0 ± 0.5	2.0 ± 0.5	2.0 ± 0.5	2.0 ± 0.5	2.0 ± 0.5	2.0 ± 0.5
Width of straggling distribution (keV) [b]	4.1 ± 0.1	7.2 ± 0.4	4.1 ± 0.1	7.2 ± 0.4	4.1 ± 0.1	7.2 ± 0.4
Target thickness (FWHM in keV)	2.1 ± 0.1	6.6 ± 0.2	2.1 ± 0.1	6.6 ± 0.2	2.1 ± 0.1	6.6 ± 0.2

[a] To a good approximation, this is the systematic uncertainty in each data point.
[b] We assume the energy dispersion and straggling to be normal distributions. Quoted values for the widths are the standard deviations of those distributions. Uncertainties quoted are the uncertainties in the standard deviations. These uncertainty distributions are also assumed to be normal distributions.

was found to be $(0.02 \pm 0.05)\%$ for ~4.4-MeV deuterons and $(0.11 \pm 0.05)\%$ for ~9-MeV α particles.

4. Electronic Effects

The electronic-count rates in this experiment were purposely kept low to avoid count-rate effects. An estimate of the electronic-count-rate losses external to the analyzer was determined in the beam-current-dependence correction and has already been discussed in Sec. V B.1.

There was a possible error due to the system used to route pulses from different detectors into the analyzer. The routing error was checked by looking for counts in the spectrum of one detector where a large peak occurred in the spectrum of another detector. The result indicated that the correction and uncertainty were negligible.

5. Analyzer Dead Time

Two methods were used to determine analyzer dead times. In the first method, the ratio of current-integrator pulses fed directly into a scaler, and current-integrator pulses counted in channel zero of the multichannel analyzer was determined. In the second method, gate pulses from the detectors counted by scalers were compared with the total number of spectrum counts for each detector in the analyzer. This ratio can be determined for all detectors. It is believed that the second method is more reliable as a determination of the analyzer dead time.

The dead time of the analyzer was typically 2% for the $^{16}O(d, \alpha)^{14}N$ reaction and 1% for the $^{14}N(\alpha, d)^{16}O$ reaction. The difference between the dead times measured by the two methods discussed above was typically 10% of the dead time.

Dead times measured for each detector by the second method agreed to within ±0.05% when there was not apparent noise in the electronics. Noisy electronics was evidenced by an excess of counts in the 100-MHz scalers above the 10-MHz scalers. This noise was usually due to the preamplifiers. If there was any doubt as to whether the dead time could be properly determined for a particular run, or if the electronics were too noisy, that run was arbitrarily omitted from the final data. Three detectors (different angles) were used in the $^{14}N(\alpha, d)^{16}O$ reaction measurements and two were used in the $^{16}O(d, \alpha)^{14}N$ reaction measurements. The uncertainty assigned to the dead-time correction was typically ±0.05%.

6. Isotopic Gas Impurities

Natural oxygen gas contains 99.76% ^{16}O, 0.04% ^{17}O, and 0.20% ^{18}O. Natural nitrogen gas contains 99.64% ^{14}N and 0.36% ^{15}N. The target densities were corrected for the percentages of ^{16}O and ^{14}N, but there is a possibility that reactions due to ^{17}O, ^{18}O, and ^{15}N will produce counts in the spectra in the same energy region as the $^{16}O(d, \alpha)^{14}N$ and $^{14}N(\alpha, d)^{16}O$ reactions. It was necessary, therefore, to measure these isotopic cross sections and correct for them. Cross sections for reactions induced by $d + {}^{17}O$, $d + {}^{18}O$, and $\alpha + {}^{15}N$ were measured by using separated isotopic gaseous targets contained within the scattering chamber by an entrance foil. The corrections based on these measurements are given in Tables I and II. The only significant correction was for the $^{14}N(\alpha, d)^{16}O$ valley region.

7. Spectrum Peak Stripping

The stripping of peaks from the spectra is related to a number of corrections already considered. Several of the scattering processes caused reaction particles to be degraded in energy: for example, slit-edge scattering, scattering in the gas, and beam-aperture scattering. Some of these energy-degraded counts should be counted, while others should not. An indication that the ideal detector peak energy distribution was nearly Gaussian in shape was obtained in the detector-efficiency experiment.[56] On the other hand, experimental peak shapes actually observed in the cross-section measurements were Gaussian on the upper side and asymmetric on the lower side with a low-energy tail.

Each process affecting the peak shape was studied in detail. An effort was made to predict and fit the observed peak shape, but this approach was found to be impractical because of the complexities of the different scattering processes. A sufficient number of channels around the spectrum peak was considered so that all true counts should have been included. Background subtraction and corrections were applied to the counts in the region and are given in Tables I and II.

E. Geometry

1. G Factor

The geometry factor G has been derived by Silverstein.[66] This relation includes the effects of the finite angular opening of the detector-slit system and the finite size of the beam. The angular distributions of the differential cross sections were carefully measured near 160° for the $^{16}O(d, \alpha)^{14}N$ reaction in order to determine the first and second derivatives of the differential cross sections which appear in Silverstein's equation.

2. Angular Uncertainty

The angle of the movable-slit system was read

from a precision angle circle with an estimated absolute uncertainty of ±3 min. The corresponding uncertainty in $\sin\theta$ at 160° was ±0.24%. However, the uncertainty in the *relative* angle between the inverse reactions was estimated to be only ±1 min.

The angular uncertainty affects the detailed-balance comparison through the cross-section dependence. This problem is considered in Sec. VII.

VI. SUMMARY OF EXPERIMENTAL RESULTS

In this section we wish to present a brief summary of the experimental cross-section measurements. Unless otherwise stated, the quoted uncertainties are the standard deviations of assumed normal distributions. The cross sections presented in this section should be understood as integrals of the true cross section weighted by the experimental energy-resolution functions. They have been corrected for all other experimental effects discussed in Sec. V.

Experimental parameters which have been measured, or estimated, for the $^{14}N(\alpha, d)^{16}O$ reaction are given in Table III. It should be repeated here that we have not established the absolute energy scale for our measurements of this reaction (see Sec. V C) to the same accuracy as in the inverse reaction.

Experimental cross sections for the $^{16}O(d, \alpha)^{14}N$ reaction are shown in Figs. 6–8, where we have plotted excitation functions measured for target-gas pressures of 0.008 and 0.024 atm. Differences in cross sections measured at different target-gas pressures are due to different energy-resolution functions. Other experimental parameters for these data are given in Table IV. The laboratory scattering angle for these data was 160°0' with an absolute uncertainty of ±3'. The uncertainty in the absolute energy scale of these measurements was ±6.7 keV. It was necessary to shift the 0.024-atm $^{16}O(d, \alpha)^{14}N$ energy scale down 7 keV to agree with the 0.008-atm $^{16}O(d, \alpha)^{14}N$ energy scale. This shift is consistent with the larger energy uncertainty associated with the greater energy loss in the higher-pressure measurements.

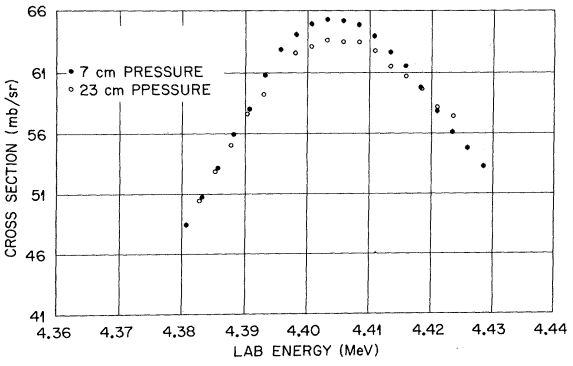

FIG. 6. Laboratory excitation functions over peak region for the $^{16}O(d, \alpha)^{14}N$ reaction for chamber gas pressures of 0.008 atm (7 cm) and 0.024 atm (23 cm). Note suppressed zero.

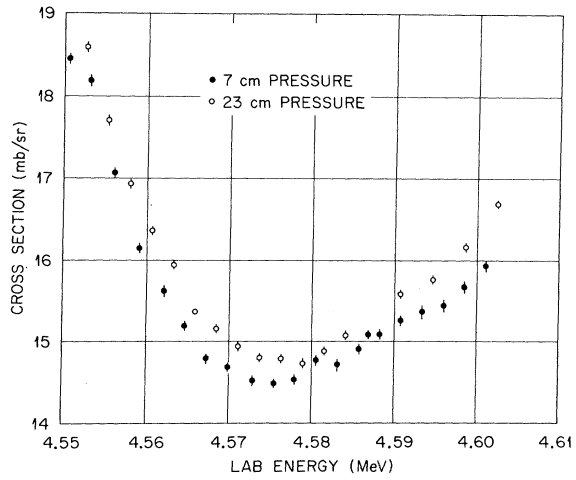

FIG. 7. Laboratory excitation functions over valley region for $^{16}O(d, \alpha)^{14}N$ reaction for chamber gas pressures of 0.008 atm (7 cm) and 0.024 atm (23 cm). Note suppressed zero.

VII. DETAILED-BALANCE COMPARISON

In this section we wish to discuss the problem of how our measured cross sections may be com-

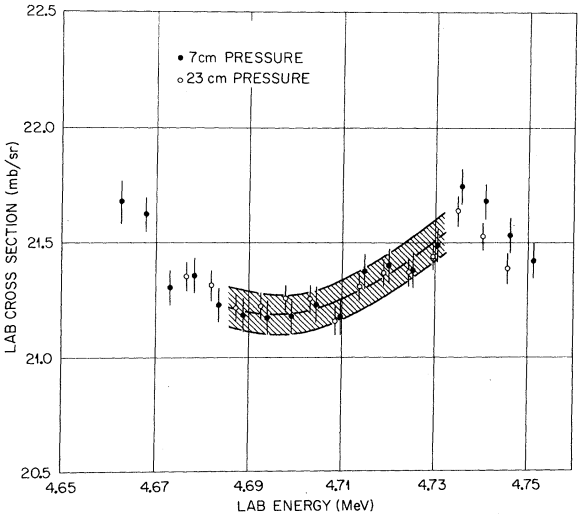

FIG. 8. Excitation functions over plateau region for $^{16}O(d, \alpha)^{14}N$ reaction for chamber gas pressures of 0.008 atm (7 cm) and 0.024 atm (23 cm). The shaded region is the result predicted for the 0.024-atm data from the 0.008-atm data. Note suppressed zero.

pared to test detailed balance. The essential difficulty is that detailed balance [Eq. (1)] relates cross sections evaluated at exact angles and energies while our measurements are weighted averages over finite intervals in both the angle and energy variables.

Let $\sigma(E, \Omega)$ be the exact differential cross section. Then in general, we measure an average cross section

$$\bar{\sigma}(E_0, \Omega_0) = \iint \sigma(E, \Omega) R(E - E_0) S(\Omega - \Omega_0) dE d\Omega , \tag{6}$$

where $R(E - E_0)$ and $S(\Omega - \Omega_0)$ are energy and angular resolution functions centered at E_0 and Ω_0, respectively.

The effect of the angular integration on the observed cross section has been treated in Sec. V E.1. This correction was made when we computed the "effective" G factor as a function of the slit-system dimensions and the angular distribution of the observed cross section. Implicit in this calculation was the assumption that the angular dependence of $\sigma(E, \Omega)$ did not vary significantly over the energy interval represented by $R(E - E_0)$. This is equivalent to the assumption that Eq. (6) may be separated into two parts,

$$\bar{\sigma}(E_0, \Omega_0) = \bar{\sigma}(E_0, \theta_0) \tag{7}$$

$$= \int \sigma(E, \theta_0) R(E - E_0) dE \tag{8}$$

and

$$\sigma(E, \theta_0) = \int \sigma(E, \Omega) S(\Omega - \Omega_0) d\Omega , \tag{9}$$

and that the operation represented by Eq. (9) is equivalent to the G-factor calculation previously performed.

We shall use the subscripts d and α to denote the incident particle, and primes to denote c.m. quantities. A typical set of measurements then consists of a single $^{14}\mathrm{N}(\alpha, d)^{16}\mathrm{O}$ cross section,

$$\bar{\sigma}_\alpha(E_{0\alpha}, \theta_{0\alpha}) = \int \sigma_\alpha(E_\alpha, \theta_{0\alpha}) R_\alpha(E_\alpha - E_{0\alpha}) dE_\alpha ,$$

and a series of $^{16}\mathrm{O}(d, \alpha)^{14}\mathrm{N}$ cross sections measured as a function of the energy,

$$\bar{\sigma}_d(E^i_{0d}, \theta_{0d}) = \int \sigma_d(E_d, \theta_{0d}) R^i_d(E_d - E^i_{0d}) dE_d .$$

We shall assume that the resolution function R^i_d is independent of i and thus drop the superscript on this variable. We also note that θ_{0d} and $\theta_{0\alpha}$ have been chosen so that the corresponding c.m. angles are equal. Therefore we will not express the angular dependence of cross sections unless necessary.

Our set of typical measurements can then be written as

$$\bar{\sigma}_\alpha(E_{0\alpha}) = \int \sigma_\alpha(E_\alpha) R_\alpha(E_\alpha - E_{0\alpha}) dE_\alpha$$

and

$$\bar{\sigma}_d(E^i_{0d}) = \int \sigma_d(E_d) R_d(E_d - E^i_{0d}) dE_d .$$

Our problem is to use these measured values, $\bar{\sigma}_\alpha(E_{0\alpha})$ and $\bar{\sigma}_d(E^i_{0d})$, to test detailed balance, which relates $\sigma'_\alpha(E_\alpha)$ and $\sigma'_d(E_d)$.

Two general techniques have been used to treat this problem. Before we discuss these in detail, we wish to discuss the assumptions which are common to both. We will consider first the absolute-comparison problem. Noting that for our case the spin factors cancel, we have from Eq. (1)

$$\sigma'_\alpha(E_\alpha)/\sigma'_d(E_d) = P_d^{\,2}/P_\alpha^{\,2} ,$$

where P_d and P_α are the c.m. momenta of the incident deuteron and α particle and E_α and E_d correspond to the same excitation energy in the compound system.

Let $\sigma'_d(E_d) = C_d \sigma_d(E_d)$; i.e., C_d is the factor which converts from the laboratory to c.m. system. The quantity χ, which we compare with unity, may then be written

$$\chi = \frac{P_d^{\,2}}{P_\alpha^{\,2}} \frac{C_d}{C_\alpha} \frac{\sigma_d(E_d)}{\sigma_\alpha(E_\alpha)}$$

$$= A \frac{\sigma_d(E_d)}{\sigma_\alpha(E_\alpha)} . \tag{10}$$

Since we did not make an accurate absolute measurement of the α-particle energy, we have inferred E_α from E_d and the reaction Q value. Thus, the factor A is considered to be a function of E_d, Q, and θ_d. In this work, we have calculated A and all other kinematic quantities with relativistically correct formulas.[67]

Equation (10) will be our starting point for absolute comparisons. For relative comparisons, we may write Eq. (10) for two different conditions.

$$\chi(E_{1d}, \theta_{1d}) = A(E_{1d}, \theta_{1d}) \frac{\sigma_d(E_{1d}, \theta_{1d})}{\sigma_\alpha(E_{1\alpha}, \theta_{1\alpha})} ,$$

$$\chi(E_{2d}, \theta_{2d}) = A(E_{2d}, \theta_{2d}) \frac{\sigma_d(E_{2d}, \theta_{2d})}{\sigma_\alpha(E_{2\alpha}, \theta_{2\alpha})} .$$

Thus the quantity to be compared with unity, ψ, is

$$\psi = \frac{\chi(E_{1d}, \theta_{1d})}{\chi(E_{2d}, \theta_{2d})} = \frac{A(E_{1d}, \theta_{1d})}{A(E_{2d}, \theta_{2d})} \frac{\sigma_d(E_{1d}, \theta_{1d})}{\sigma_d(E_{2d}, \theta_{2d})} \frac{\sigma_\alpha(E_{2\alpha}, \theta_{2\alpha})}{\sigma_\alpha(E_{1\alpha}, \theta_{1\alpha})} . \tag{11}$$

A. Weighted-Resolution-Function Method

We will now describe the first technique used for the actual cross-section comparison. Since E_α and E_d are related in a specific way, Eq. (10) can be written

$$\chi(E_d)\sigma_\alpha(E_d) = A(E_d)\sigma_d(E_d), \tag{12}$$

for any value of E_d. For any well-behaved weighting function $R(E_d)$ we have

$$\int \chi(E_d)\sigma_\alpha(E_d)R(E_d)dE_d = \int A(E_d)\sigma_d(E_d)R(E_d)dE_d . \tag{13}$$

Now we identify $R(E_d)$ with the energy-resolution function for the $^{14}\mathrm{N}(\alpha, d)^{16}\mathrm{O}$ reaction, $R_\alpha(E_\alpha)$, except that we write it here as a function of E_d. Furthermore, we note that to a good approximation we may form a weighted sum of the deuteron energy-resolution functions, which are equivalent to $R_\alpha(E_d)$.

$$R_\alpha(E_d) = \sum_{i=1}^{n} w_i R_d(E_d^i) . \tag{14}$$

Now let E_{0d} be the center energy of $R_\alpha(E_d)$. We note that $A(E_d)$ has only a small linear energy dependence. Since $\sigma_\alpha(E_d)$ and $R_\alpha(E_d)$ are approximately symmetric with respect to E_{0d} for each of the cases studied, it is a good approximation to remove $A(E_d)$ from the integration and replace it by $A(E_{0d})$. Thus we may rewrite Eq. (13) as

$$\int \chi(E_d)\sigma_\alpha(E_d)R_\alpha(E_d)dE_d = A(E_{0d})\sum_{i=1}^{n} w_i \int \sigma_d(E_d)R_d(E_d^i)dE_d . \tag{15}$$

Now we *define* $\bar{\chi}(E_{0d})$ by the relation

$$\bar{\chi}(E_{0d}) \equiv \frac{\int \chi(E_d)\sigma_\alpha(E_d)R_\alpha(E_d)dE_d}{\int \sigma_\alpha(E_d)R_\alpha(E_d)dE_d} . \tag{16}$$

Then from Eqs. (8), (15), and (16) we have

$$\bar{\chi}(E_{0d}) = A(E_{0d})\sum_{i=1}^{n} w_i \bar{\sigma}_d(E_{0d}^i)/\bar{\sigma}_\alpha(E_{0d}) . \tag{17}$$

This is the fundamental relation which we will use for our cross-section comparison. It should be particularly noted that $\bar{\chi}(E_{0d})$ is an average value of $\chi(E_d)$ weighted by both $R_\alpha(E_d)$ and $\sigma_\alpha(E_d)$.

In order to use Eq. (17) it is necessary to know the coefficients w_i, which in turn requires a knowledge of the resolution functions R_α and R_d. We will assume that R_α and R_d are the convolution of three factors: energy loss by the beam in the target volume, beam energy straggling in the gas preceding the target volume, and the "intrinsic" energy resolution of the beam as it enters the scattering chamber. As stated above, we will assume that the intrinsic energy resolution of the beam and the beam-energy straggling are normal distributions with widths as given in Tables III and IV. To a good approximation the energy loss function, considered as a function of position along the beam axis, is a symmetric trapezoidal function whose full width at half maximum is also given in Tables III and IV. It should be noted that these widths are not known exactly and that the uncertainty in these widths contributes substantially to the uncertainty in some of the final detailed-balance comparisons. We will discuss this problem in detail below.

Given specific values of the various resolution-function widths, the coefficients w_i were calculated in a straightforward way. Specifically, we calculated the convolved functions $R_\alpha(E_d)$ and $R_d(E_d)$ numerically and then used a least-squares computer program to find w_i by minimizing the sum

$$\sum_{j=1}^{m} [R_\alpha(E_d^j) - \sum_{i=1}^{n} w_i R_d(E_d^j)]^2 ,$$

where E_d^j were the arguments (typically 100) for which R_α has been numerically evaluated. In this calculation R_d was approximated by a normal distribution. In order to minimize statistical uncertainty in the sum $\sum_{i=1}^{n} w_i\sigma_d(E_{0d}^i)$, and thus in $\bar{\chi}(E_{0d})$ we imposed the additional constraint $w_i \geq 0$. In general, the fit of $\sum_{i=1}^{n} w_i R_d(E_d)$ to $R_\alpha(E_d)$ was very good and we believe that a negligible uncertainty is introduced into $\bar{\chi}(E_{0d})$ by the fitting procedure.

In a more general sense, there are uncertainties in w_i because of uncertainties in $R_d(E_d)$ and $R_\alpha(E_d)$ and in E_{0d} (the energy at which $\bar{\sigma}_\alpha$ was measured with respect to the set E_{0d}^i). However, these uncertainties are correlated and we calculated the effect of these uncertainties by considering their effect directly on $\bar{\chi}(E_{0d})$.

Once the set w_i had been determined $\bar{\chi}(E_{0d})$ was calculated easily, since the other quantities in Eq. (17) were known (e.g., Tables III and IV, Figs. 6–8). Estimating the uncertainty in $\bar{\chi}(E_{0d})$ was a more difficult problem. To show how these estimates were made, we will now discuss our assumptions in detail. Table V is a tabulation of the results of these assumptions.

1. Statistical uncertainties. We assumed that the statistical uncertainties $\Delta\sigma_i$ associated with $\bar{\sigma}_d(E_{0d}^i)$ were uncorrelated. Since w_i are assumed to have negligible associated uncertainty, the statistical uncertainty in the sum $\sum_{i=1}^{n} w_i\bar{\sigma}_d(E_{0d}^i)$ is just $(\sum_{i=1}^{n} w_i^2\Delta\sigma_i^2)^{1/2}$. This is the quantity given in Table V under the heading (d, α) statistics.

2. Systematic uncertainties. We assumed that the

TABLE V. Summary of uncertainties (in percent) for absolute comparison of (d,α) and (α,d) cross sections.

Source	(d,α) pressure = 0.008 atm Peak	Valley	Plateau	(d,α) pressure = 0.024 atm Peak	Valley	Plateau
(α,d) statistics	±0.327	±0.411	±0.278	±0.327	±0.411	±0.278
(d,α) statistics	±0.082	±0.133	±0.130	±0.086	±0.130	±0.113
(α,d) systematic	±0.325	±0.353	±0.300	±0.325	±0.353	±0.300
(d,α) systematic	±0.277	±0.285	±0.283	±0.224	±0.247	±0.238
$A(E_{0d}, \theta_d, Q)$	±0.098	±0.093	±0.089	±0.098	±0.093	±0.089
Relative energy	−0.175, −0.194	+0.260, +0.212	+0.345, −0.224	−0.169, −0.174	+0.243, +0.335	+0.279, −0.138
Relative angle	±0.061	±0.038	±0.011	±0.061	±0.038	±0.011
(d,α) energy-resolution function	+0.126, −0.097	+0.057, −0.073	+0.002, −0.003	+0.377, −0.294	+0.225, −0.297	+0.009, −0.010
(α,d) energy-resolution function	+0.806, −1.129	+0.676, −0.441	+0.031, −0.021	+0.758, −1.051	+0.815, −0.551	+0.037, −0.026
Combined uncertainty	+0.987, −1.276	+0.958, −0.776	+0.626, −0.568	+1.000, −1.226	+1.075, −0.879	+0.569, −0.514

systematic uncertainties in $\bar{\sigma}_d(E^i_{0d})$ were completely correlated. (This is the most conservative assumption.) Then the systematic uncertainty in $\sum_{i=1}^{n} w_i \bar{\sigma}_d(E^i_{0d})$ will be equal to the systematic uncertainty in a single measurement $\bar{\sigma}_d(E^i_{0d})$.

3. Uncertainties in energy and angle. Two kinds of uncertainties may occur. First, there are uncertainties in the absolute deuteron bombarding energy and (d, α) scattering angle. These affect the detailed-balance comparison [Eq. (17)] only through the factor $A(E_{0d})$. Second, there are uncertainties in the correspondence of the (d, α) and (α, d) bombarding energies and angles. We will consider these problems separately.

As we have noted above, $A(E_{0d})$ is a function of E_{0d}, θ_d, and Q. For our absolute comparisons, we took $Q = 3.110\,22 \pm 0.000\,38$ MeV, $\theta_d = 160°0' \pm 3'$, and

$$E_{0d} = \begin{cases} 4.4052 \pm 0.0067 \text{ MeV} & \text{(peak)} \\ 4.5775 \pm 0.0067 \text{ MeV} & \text{(valley)} \\ 4.7100 \pm 0.0067 \text{ MeV} & \text{(plateau)}. \end{cases}$$

The uncertainty in A caused by each of these factors was determined numerically. The total uncertainty in A was determined by combining these individual contributions in quadrature with the results tabulated in Table V under the heading $A(E_{0d}, \theta_d, Q)$.

TABLE VI. Results of detailed-balance comparisons by two methods for absolute ratio.

Comparison	Weighted resolution function	Likelihood function
Peak (0.008 atm)	$0.9914^{+0.0099}_{-0.0128}$	0.9901 ± 0.0115
Peak (0.024 atm)	$0.9858^{+0.0100}_{-0.0123}$	0.9904 ± 0.0115
Valley (0.008 atm)	$1.0053^{+0.0096}_{-0.0078}$	1.0055 ± 0.0076
Valley (0.024 atm)	$1.0111^{+0.0107}_{-0.0088}$	1.0065 ± 0.0084
Plateau (0.008 atm)	$0.9994^{+0.0063}_{-0.0057}$	
Plateau (0.024 atm)	$0.9991^{+0.0057}_{-0.0051}$	
Peak (combined)	$0.9886^{+0.0096}_{-0.0123}$	
Valley (combined)	$1.0082^{+0.0099}_{-0.0079}$	
Plateau (combined)	$0.9992^{+0.0052}_{-0.0048}$	

The effect of uncertainties in the relative bombarding energy was estimated by repeating the determination of w_i for different assumed values of E_{0d} and then calculating $\bar{\chi}(E_{0d})$ with these w_i. These uncertainties [in $\bar{\chi}(E_{0d})$] are listed in Table V under Relative Energy. They represent the effect of the uncertainties in E_{0d} listed in Table III. For the peak and valley regions an attempt was made to experimentally make E_{0d} correspond to the maximum and minimum cross section, respectively. Any deviation of the true E_{0d} from the intended E_{0d} makes $\bar{\chi}(E_{0d})$ go down for the peak and up for the valley. This is the reason, for example, that two negative values are quoted in Table V for the peak region. These two values correspond to changes in E_{0d} of +2 keV and −2 keV, respectively.

As stated above we have assumed that the angular dependence of the cross section does not vary significantly over the energy interval represented by $R_\alpha(E_d)$. Under this assumption, uncertainties in $\bar{\chi}(E_{0d})$ due to uncertainties in the relative scattering angle $\pm\Delta\theta$ are given by

$$[\partial \bar{\sigma}_d(E_{0d})/\partial\theta](\pm\Delta\theta).$$

This was determined in our case by measuring angular distributions at 1° intervals at the appropriate bombarding energies. The effect on $\bar{\chi}(E_{0d})$ due to relative-angle uncertainties of ±1 min are given in Table V under Relative angle.

4. Uncertainties in $R_\alpha(E_d)$ and $R_d(E_d)$. Uncertainties in R_α and R_d cause uncertainties in $\bar{\chi}(E_{0d})$ by introducing correlated uncertainties into the determination of w_i. Estimates of uncertainties in the individual components of R_α and R_d are given in Tables III and IV. Their effect on $\bar{\chi}(E_{0d})$ was

estimated by repeating the sequence of calculations which has been described. That is, R_α or R_d was recalculated using different parameters for the functions to be convolved, w_i were determined using the new resolution function, and $\bar{\chi}(E_{0d})$ was calculated using Eq. (17). Changes in $\bar{\chi}(E_{0d})$ corresponding approximately to changes of one standard deviation in the individual components of R_α and R_d are given in Table V under the headings (d, α) Energy-resolution function and (α, d) Energy-resolution function.

5. *Combined uncertainty*. What one would like to have as the result of an experiment of this type is the so-called likelihood function, i.e., the probability that a given $\bar{\chi}(E_{0d})$ is the correct $\bar{\chi}(E_{0d})$ given as a function of $\bar{\chi}(E_{0d})$. The problem in the present analysis is that $\bar{\chi}(E_{0d})$ is a nonlinear function of the measured quantities; for example, the relative bombarding energy. The essential assumptions of this first method are that we may estimate the standard deviation of the likelihood function for a given comparison by combining the positive and negative individual contributions in quadrature and that the standard deviations calculated in this way correspond to a confidence interval of 68%. For example, in Table V the value of −1.276% given as one limit of the combined uncertainty in the first column is the root-mean-square of all the negative values in that column, including an average uncertainty of −0.185% for relative energy. This assumption is based on the idea that the individual sources of uncertainty are uncorrelated and are reasonably well approximated by normal distributions.

A summary of the absolute-comparison results is given in Table VI for (d, α) pressures of 0.008-, 0.024-, and for the 0.008- and 0.024-atm data combined. By the latter, we mean

$$\bar{\chi}(E_{0d})|_{\text{combined}} = \tfrac{1}{2}\bar{\chi}(E_{0d})|_{0.008\ \text{atm}} + \tfrac{1}{2}\bar{\chi}(E_{0d})|_{0.024\ \text{atm}} .$$

In the uncertainty calculations for the combined data, we assumed that 0.008- and 0.024-atm uncertainties for the (d, α) energy-resolution function, relative bombarding energy (valley region), (d, α) statistics, and (d, α) systematic effects were uncorrelated. Since there is no reason to believe that the high- or low-pressure data are more accurate, we will use as our final answer the combined comparison.

A sensitive test of the comparison procedure we have just described is a comparison of the 0.008- and 0.024-atm (d, α) data. In particular, the 0.008- and 0.024-atm (d, α) cross sections have substantially different energy-resolution functions (see Table IV). Thus we can consider a problem analogous to Eq. (17) where $\bar{\sigma}_\alpha(E_{0d})$ and $\bar{\sigma}_d(E^i_{0d})$ are replaced by the 0.024- and the 0.008-atm (d, α) cross sections, respectively. In this case, $A(E_{0d}) = 1$, but in all other respects the problem is similar except that we know the desired answer; i.e., $\bar{\chi}(E_{0d}) = 1$.

We have performed such a comparison with the results shown in Figs. 8–10. Rather than calculate a ratio of cross sections, we have calculated the 0.024-atm cross section as predicted from the 0.008-atm cross sections. These are shown in Figs. 8–10 as crosshatched bands. The center line of these bands is the predicted value and the edges represent a 68% confidence interval calculated in the same way as for the detailed-balance comparison. In this uncertainty calculation no relative-angle uncertainty was assumed (since the detector was not moved) and no relative-energy uncertainty was assumed, since the comparisons are made as a function of relative energy. Although these comparisons are not perfect for the peak (Fig. 9) and valley (Fig. 10), they are consistent with the estimated uncertainties. As can be seen in Fig. 8, the comparison for the plateau region is quite good. This is gratifying, since it is the plateau region which provides our most

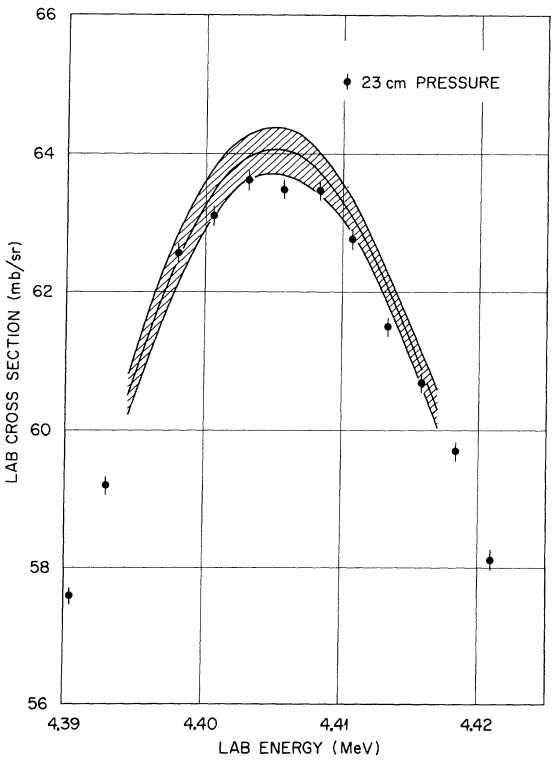

FIG. 9. Excitation function over the peak region for the $^{16}O(d, \alpha)^{14}N$ reaction showing 0.024-atm (23 cm) data points and the 0.024-atm data predictions (shaded region) calculated from the 0.008-atm data. Note suppressed zero.

sensitive detailed-balance comparison.

Since our data consist of cross-section measurements at three different compound-nucleus energies, they can also be combined to form three relative-energy comparisons of detailed balance. The quantity which we wish to compare with unity, ψ, is defined in Eq. (11). However, we again have the problem that our measured cross sections are integrals of the true cross section weighted by experimental energy-resolution functions. The resolution of this problem proceeds just as before. Rather than repeat the entire development we will *define* our average $\overline{\psi}$ by

$$\overline{\psi}(E_{1d}, E_{2d}) = \overline{\chi}(E_{1d})/\overline{\chi}(E_{2d}), \tag{18}$$

where $\overline{\chi}(E_{1d})$ and $\overline{\chi}(E_{2d})$ are defined by Eq. (16) and calculated by Eq. (17). We have dropped the angular dependence of Eq. (11), since for our data $\theta_{1d} = \theta_{2d}$.

$\overline{\chi}(E_{1d})$ and $\overline{\chi}(E_{2d})$ are the absolute ratios we have previously calculated (Table VI) and the calculation of $\overline{\psi}(E_{1d}, E_{2d})$ proceeds directly. Calculation of the uncertainty in $\overline{\psi}(E_{1d}, E_{2d})$ is more complicated, since some sources of uncertainty for the two (α, d) and two (d, α) measurements in a relative ratio will be correlated. For example, $\overline{\psi}(E_{1d}, E_{2d})$ contains the ratio $\overline{\sigma}_\alpha(E_{2d})/\overline{\sigma}_\alpha(E_{1d})$, and systematic uncertainties which are common to both $\overline{\sigma}_\alpha(E_{2d})$ and $\overline{\sigma}_\alpha(E_{1d})$ will tend to cancel. In order to estimate uncertainties in the values of $\overline{\psi}(E_{1d}, E_{2d})$ to be reported, we have made the approximation that the following sources of systematic uncertainty (see Tables I and II) cancel completely for both pairs of (α, d) and (d, α) measurements: Faraday-cup ionization, beam-current dependence, slit-edge scattering, detector inefficiency, beam-scattering loss, compensation, and secondary-electron suppression. In addition, uncertainties introduced in the determination of w_i for the measurements centered at the peak and valley are correlated, but in a way which increases the total uncertainty. In particular, a change in either R_d or R_α causes the sum $\sum_{i=1}^{n} w_i \overline{\sigma}_d(E_{0d}^i)$ to change in opposite directions at the peak and valley. Thus, uncertainty contributions due to R_d and R_α must be added for the peak/valley comparison.

Table VII summarizes the results of relative-energy comparisons calculated with the combined 0.008- and 0.024-atm (d, α) cross-section data. The uncertainties quoted in this table were calculated in the same way as those for the absolute comparisons, with the additional changes noted above.

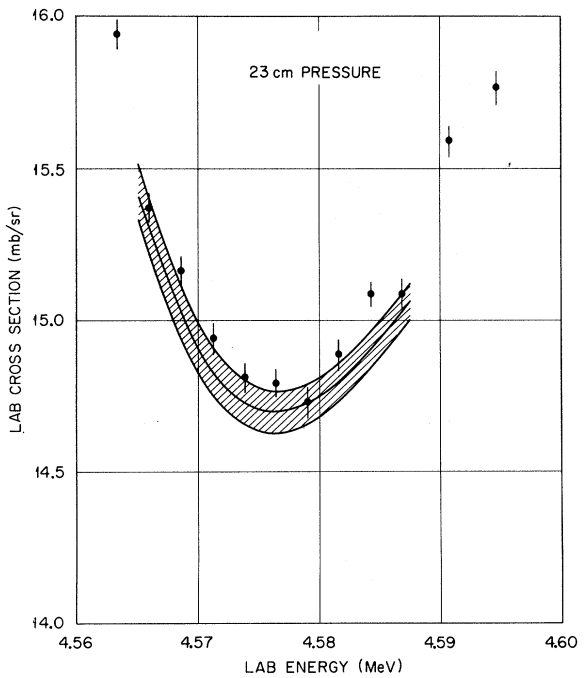

FIG. 10. Excitation function over the valley region for the $^{16}O(d, \alpha)^{14}N$ reaction showing 0.024-atm (23 cm) data points and the 0.024-atm data predictions (shaded region) calculated from the 0.008-atm data. Note suppressed zero.

B. Likelihood-Function Method

Another approach to the comparison problem was made employing the technique of likelihood inference.[68] Given the data measured in the experiment and a set of assumptions, this method of analysis computes a likelihood or "probability" for every value of the parameter $\chi = (\sigma_{d,\alpha}/\sigma_{\alpha,d}) \times A$. If detailed balance holds, this likelihood function, $\mathcal{L}(\chi)$, would be a peak centered about 1.0 with a width which is a measure of the uncertainty in the experiment. In general, this peak is non-Gaussian.

If a series of n measurements are made of a quantity γ, and if the probability distribution (or probability density) of measuring a particular value of γ is given by $f(\gamma, \mu)$, where μ is a mean value of an infinite number of measurements of γ (μ is not known), then the likelihood function is defined as

$$\mathcal{L}(\mu) = \prod_{i=1}^{n} f(\gamma_i, \mu). \tag{19}$$

TABLE VII. Summary of relative energy-comparison results. Values of $\psi(E_{1d}, E_{2d})$ as defined in text.

$\psi(E_{\text{peak}}, E_{\text{valley}})$	$0.9806^{+0.0152}_{-0.0202}$
$\psi(E_{\text{peak}}, E_{\text{plateau}})$	$0.9894^{+0.0105}_{-0.0132}$
$\psi(E_{\text{valley}}, E_{\text{plateau}})$	$1.0090^{+0.0108}_{-0.0086}$

$\mathfrak{L}(\mu)$ is a probability or creditability calculated from the data points and is dependent on the assumed form of the probability density. Except for arbitrary normalization, likelihood functions can be treated much like probability functions, i.e., they can be multiplied to form joint likelihoods, and they can be integrated over variables that are to be eliminated.

We will be concerned first with the (d, α) measurements. The likelihood of inferring a particular functional form of an averaged cross section $\bar{\sigma}_{d_0}(E)$ from a series of cross-section measurements $[\bar{\sigma}_d(E_{d_1}), \bar{\sigma}_d(E_{d_2}), \ldots, \bar{\sigma}_d(E_{d_i}), \ldots, \bar{\sigma}_d(E_{d_n})]$, where the distribution of cross-section measurements is assumed to be normal with uncorrelated standard deviations of $[s_1, s_2, \ldots, s_i, \ldots, s_n]$ and a correlated uncertainty of γ_d, can be written as the integral over all values of systematic error K_d of the likelihood of inferring $\bar{\sigma}_{d_0}(E)$ from the set of data points (assuming a K_d) multiplied by the probability of a particular K_d,

$$l_d(\bar{\sigma}_{d_0}(E)) = \int_{-\infty}^{\infty} dK_d \left\{ \frac{1}{\sqrt{2\pi}\,\gamma_d} \exp\left[-\frac{(K_d - 1)^2}{2\gamma_d{}^2} \right] \right\} \times \prod_{i=1}^{n} \left(\frac{1}{\sqrt{2\pi}\,s_i} \exp\left\{ -\frac{[K_d \bar{\sigma}_d(E_{d_i}) - \bar{\sigma}_{d_0}(E_{d_i})]^2}{2s_i{}^2} \right\} \right), \tag{20}$$

where K_d is assumed to be normally distributed with a standard deviation γ_d.

This integration has the effect of including the uncertainty of K_d into $l_d(\bar{\sigma}_{d_0}(E))$ in terms of the set of data and γ_d. This technique; i.e., of integrating a likelihood function over a variable weighted by a probability density of that variable; will be used frequently in this development.

At this point we will make an assumption about the functional form of $\sigma_d(E)$ and therefore about $\bar{\sigma}_{d_0}(E)$. We will assume that $\sigma_d(E)$ can be represented in the region of the set of data as a power series in E up to E^3 of the form:

$$\sigma_d(E) = a_d(1 + C_{1d}E + C_{2d}E^2 + C_{3d}E^3). \tag{21}$$

The consequences of this assumption will be discussed later. Then

$$\bar{\sigma}_{d_0}(E) = \int_{-\infty}^{\infty} R(E-\delta)\sigma_d(\delta)d\delta = a\{1 + C_{1d}E + C_{2d}[E^2 + M_{d2}] + C_{3d}[E^3 + 3EM_{d2}]\}, \tag{22}$$

where $M_{d2} = \int_{-\infty}^{\infty} R(x)x^2dx$, the second moment of the resolution function, and it is necessary to use the assumption that $R(x)$ is symmetric about $x = 0$ and that $\int_{-\infty}^{\infty} R(x)dx = 1$. The above expression gives us the means of parametrizing $\bar{\sigma}_{d_0}(E)$, the integrated cross section, in terms of parameters of the discrete cross section $\sigma_d(E)$ (i.e.: a_d, C_{1d}, C_{2d}, and C_{3d}) and a single parameter, M_{d2}, of the resolution function. This functional form has two advantages. First of all we are not forced to assume very much about $R(x)$, and secondly, we are able to obtain a particularly simple expression for the detailed-balance parameter χ if we assume, as previously discussed, that a violation of detailed balance would not change the shape of the discrete cross section, only its amplitude; i.e.,

$$\chi = A\sigma_{d,\alpha}/\sigma_{\alpha,d} = Aa_d/a_\alpha . \tag{23}$$

Putting the expression for $\bar{\sigma}_{d_0}$ into $l_d(\bar{\sigma}_{d_0}(E))$ we obtain an expression for $l_d(a_d, C_{1d}, C_{2d}, C_{3d}, M_{d2})$. In order to include the uncertainty in M_{d2} we integrate the likelihood function over all possible values of the second moment of the resolution function

$$l_d(a_d, C_1, C_2, C_3) = \int_{-\infty}^{\infty} dM_{d2} P_{M_{d2}} \times l(a_d, C_{1d}, C_{2d}, C_{3d}, M_{d2}), \tag{24}$$

where $P_{M_{d2}}$ is the probability of having a particular M_{d2} and we have assumed this to be a normal distribution about the calculated second moment of the resolution function.

As mentioned previously, we decided to convert the (α, d) measurements into the (d, α) laboratory frame of reference. Consequently, the (α, d) measurement should be represented as $\bar{\sigma}_\alpha(E + E_0)$, where E_0 is the systematic error in the energy of the (α, d) measurement relative to the (d, α) measurements. The experiment has been performed in such a way as to make $E_0 = 0$, but uncertainties in all energy measurements contribute to a probability, which we will assume to be Gaussian, of E_0 being any value around zero.

Except for the additional parameter E_0 we can construct $l_\alpha(a_\alpha, C_1, C_2, C_3, E_0)$ in the same way as we constructed the (d, α) likelihood function. Then the likelihood $\mathfrak{L}(\chi)$ that a given detailed-balance parameter χ can be inferred from the (α, d) and (d, α) sets of data is given by

$$\mathfrak{L}(\chi) = \int dE_0 P_{E_0} \int da_d \int dC_3 \int dC_2 \int dC_1 \times l_d(a_d, C_1, C_2, C_3) l_\alpha(Aa_d/\chi, C_1, C_2, C_3), \tag{25}$$

where P_{E_0} is the probability density of E_0, which was assumed to be a Gaussian with a mean of $E_0 = 0$ and a standard deviation equal to the uncertainty in the relative-energy measurements.

The integration over C_1 can be done in closed

form, but the remaining four integrals must be done numerically. The limits of the range of numerical integration for the integrals over C_2, C_3, and a_d were determined by doing a least-squares fit of each set of the (d, α) data to Eq. (22) and then choosing the limits to be one standard deviation on either side of the best-fit values. This procedure also tested the assumption that the data could be parametrized in the functional form of Eq. (22), which is equivalent to the assumption that the cross section over the region of a set of data can be expressed as a power series in the energy up to E^3 [Eq. (21)]. For every set of data, the cross-section measurements near the edges of the energy range were neglected so as to restrict the energy region to be analyzed in order to make the assumption of the cubic form of the cross section more valid. In general the χ^2 values for these fits normalized to the number of degrees of freedom were good; however, the results for the 0.024-atm sets of data were not as good as those for the 0.008-atm sets of data.

A computer program was written to calculate $\mathfrak{L}(\chi)$ for the comparison of two sets of data. In order to check the program, the mathematical development of $\mathfrak{L}(\chi)$, and the internal consistency of the (d, α) data, this program was used to determine $\mathfrak{L}(\sigma_{d,\alpha}(0.008\text{ atm})/\sigma_{d,\alpha}(0.024\text{ atm}))$ for the peak and valley regions. The likelihood function calculated in this manner for a comparison of the two sets of (d, α) data measured on the "peak" appears in Fig. 11. This likelihood function, as with the others calculated, tends to peak about 1.0; the width of the peak is an indication of the uncertainty of the comparison. The secondary peak that appears in Fig. 11 is the only one that was observed during the analysis of this experiment. Figure 12 shows the likelihood function $\mathfrak{L}(\sigma_{d,\alpha}(0.008\text{ atm})/\sigma_{\alpha,d})$ calculated for the comparison between the 0.008-atm (d, α) data and the (α, d) data in the valley.

Attempts to analyze the plateau data with the same computer program proved unsuccessful because of computational difficulties which resulted in computer underflows. It was decided to limit the likelihood-function analysis to the peak and valley rather than to try to develop new numerical techniques.

The uncertainties quoted in the likelihood are all symmetric about the most likely value and are as a whole slightly smaller than those derived by the

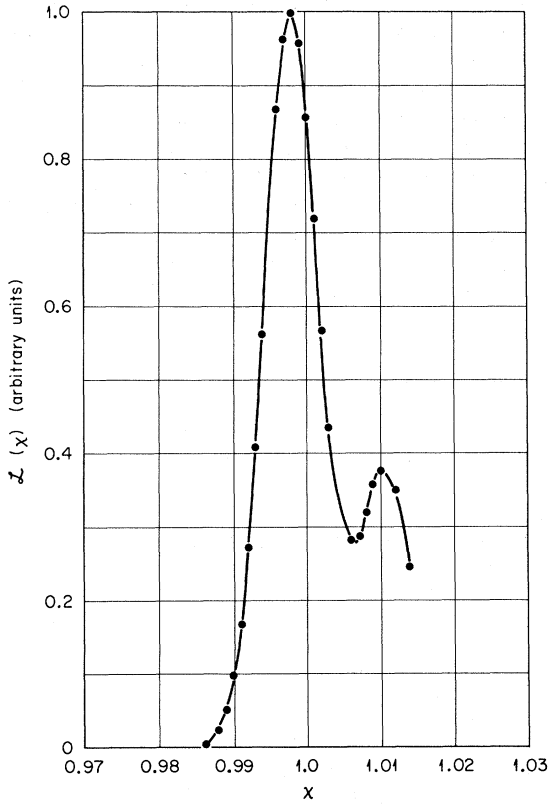

FIG. 11. Comparison of absolute ratio of σ_d for the 0.008- and 0.024-atm peak data calculated using the likelihood-function method.

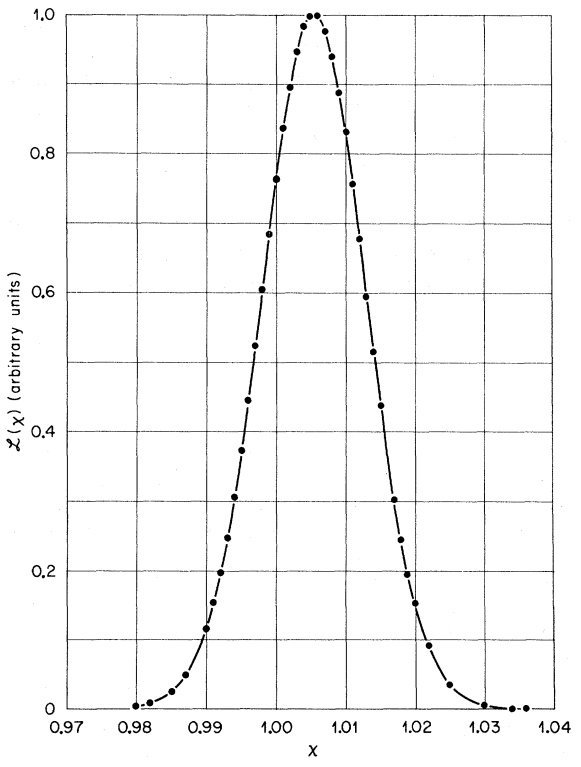

FIG. 12. Comparison of absolute ratio of σ_d (0.008 atm) with the σ_α valley data using the likelihood-function method.

other analysis. The likelihood uncertainties are symmetric because the formalism that was developed assumed that all contributing uncertainties were in the form of variances of assumed normal distributions, when in fact we do not know, nor do we have any way of knowing, the distribution of many uncertainties in the experiment. Perhaps the likelihood uncertainties are smaller because in general the energy range over which (d, α) data was analyzed for each set was smaller; however, the difference between the two sets of uncertainties can hardly be called significant.

These results of the likelihood analysis provided us with an independent check on the comparison of the (α, d) and (d, α) measurements. This type of approach to the analysis of a precision experiment should be encouraged.

VIII. CONCLUSION

As shown in Table VI, detailed balance is satisfied to within our experimental uncertainty, which ranges from ±0.4 to ±1.1%. Our best results of ±0.4 to ±0.5% are obtained for the plateau region.

In general, we would like to use these results to place a limit on the fraction of the Hamiltonian which is T noninvariant. Several authors[44-52] have attempted to relate limits on detailed balance to the properties of the corresponding Hamiltonians, but their results are model dependent and in some cases do not agree. Since our reaction is not a direct reaction and since we probably are not in the statistical-fluctuation region, we have not attempted to use the presently available theoretical results to calculate the T-noninvariant fraction of the Hamiltonian. Our reaction is probably in the region of a few overlapping levels, and the calculation by Mahaux and Weidenmüller[46] for the two-level case may be appropriate. They conclude that a T violation could be greatly enhanced in this case. Moldauer[52] has calculated the T-odd part of the Hamiltonian H for three recent detailed-balance experiments. He calculates $\langle H_{\text{odd}} \rangle$ less than 27 keV for the experiment of Weitkamp *et al.*[30] and at most 50 eV for the experiments of von Witsch, Richter, and von Brentano[31] and the present one. The reaction[30] studied by Weitkamp *et al.*, $^{24}\text{Mg}(d,p)^{25}\text{Mg}$, proceeds primarily as a direct reaction and the von Witsch, Richter, and von Brentano[31] reaction, $^{24}\text{Mg}(\alpha,p)^{27}\text{Al}$, was measured in the region of fluctuating cross sections.

A more modest goal is the idea of relating a violation in detailed balance to the fractions of the reaction amplitudes which are T noninvariant. Again, this is a model-dependent procedure and depends sensitively on the phase angles Φ_i between the T-even, f_i^e, and T-odd, f_i^o, parts of the amplitudes. In the absence of specific information, we have adopted what has become a standard technique in experiments of this type. That is, we assume for each amplitude that $f_i^o \ll f_i^e$ and Φ_i is unknown. By allowing Φ_i to assume random values, we can then calculate an average relation between the limit on detailed balance and the fractional values of f_i^o.

In the present case, two independent amplitudes may make substantial contributions to the reaction cross section. For various reasonable assumptions about the relative value of f_1^o and f_2^o, we estimate that the limit placed on the T-odd part of the amplitudes is about twice as good as the limit placed on detailed balance. Thus our best upper limit for the T-odd fraction of the reaction amplitudes is 0.2%.

---

†Research sponsored by the U. S. Atomic Energy Commission under contract with Union Carbide Corporation.

*Oak Ridge Graduate Fellow from the University of Tennessee under appointment by Oak Ridge Associated Universities. Present address: University of Virginia, Charlottesville, Virginia.

‡U. S. Atomic Energy Commission Postdoctoral Fellow under appointment from Oak Ridge Associated Universities. Present address: Bell Telephone Laboratory, Holmdel, New Jersey.

§Present address: Case Western Reserve University, Cleveland, Ohio.

[1]J. H. Christenson, J. W. Cronin, V. L. Fitch, and R. Turlay, Phys. Rev. Letters 13, 138 (1964).

[2]T. D. Lee, Phys. Today 19, 23 (1966).

[3]L. Wolfenstein, Phys. Rev. Letters 13, 562 (1964).

[4]T. D. Lee and L. Wolfenstein, Phys. Rev. 138, B1490 (1965).

[5]J. M. Gaillard, F. Krienen, W. Galbraith, A. Hussri, M. R. Jane, N. H. Lipman, G. Manning, T. Ratcliffe, P. Day, A. G. Parham, B. T. Payne, A. C. Sherwood, H. Faissner, and H. Reithler, Phys. Rev. Letters 18, 20 (1967).

[6]J. W. Cronin, P. F. Kunz, W. S. Risk, and P. C. Wheeler, Phys. Rev. Letters 18, 25, 152(E) (1967).

[7]J. Prentki and M. Veltman, Phys. Letters 15, 88 (1965).

[8]J. Bernstein, G. Feinberg, and T. D. Lee, Phys. Rev. 139, B1650 (1965).

[9]C. S. Wu, E. Ambler, R. W. Hayward, D. D. Hoppes, and R. P. Hudson, Phys. Rev. 105, 1413 (1957).

[10]M. T. Burgy, V. E. Krohn, T. B. Novey, G. R. Ringo, and V. L. Telegdi, Phys. Rev. 120, 1829 (1960); Phys. Rev. Letters 1, 324 (1958).

[11]M. A. Clark and J. M. Robson, Can. J. Phys. 38, 693 (1960); 39, 13 (1961).

[12]B. G. Erozolimsky, L. N. Bondarenko, Y. A. Mostovoy, B. A. Obinyakov, V. P. Zacharova, and V. A. Titov, Phys. Letters 27B, 557 (1968).
[13]F. P. Calaprice, E. D. Commins, H. M. Gibbs, G. L. Wick, and D. A. Dobson, Phys. Rev. Letters 18, 918 (1967); Phys. Rev. 184, 1117 (1969).
[14]E. Fuschini, V. Gadjokov, C. Maroni, and P. Veronesi, Nuovo Cimento 33, 709, 1309 (1964).
[15]J. Kajfosz, J. Kopecký, and J. Honzátko, Phys. Letters 20, 284 (1966).
[16]O. C. Kistner, Phys. Rev. Letters 19, 872 (1967).
[17]M. Atac, B. Chrisman, P. Debrunner, and H. Frauenfelder, Phys. Rev. Letters 20, 691 (1968).
[18]E. Zech, F. Wagner, H. J. Körner, and P. Kienle, in *Hyperfine Structure and Nuclear Radiations*, edited by E. Matthias and D. A. Shirley (North-Holland Publishing Company, Amsterdam, The Netherlands, 1968), p. 314.
[19]R. B. Perkins and E. F. Ritter, Phys. Rev. 174, 1426 (1968).
[20]C. L. Oxley, W. F. Cartwright, J. Rouvina, E. Baskir, D. Klein, J. Ring, and W. Skillman, Phys. Rev. 91, 419 (1953).
[21]P. Hillman, A. Johansson, and G. Tibell, Phys. Rev. 110, 1218 (1958).
[22]A. Abashian and E. M. Hafner, Phys. Rev. Letters 1, 255 (1958).
[23]L. Rosen and J. E. Brolley, Jr., Phys. Rev. Letters 2, 98 (1959).
[24]C. F. Hwang, T. R. Ophel, E. H. Thorndike, and R. Wilson, Phys. Rev. 119, 352 (1960).
[25]D. G. McDonald, W. Haeberli, and L. W. Morrow, Phys. Rev. 133, B1178 (1964).
[26]E. E. Gross, J. J. Malanify, A. van der Woude, and A. Zucker, Phys. Rev. Letters 21, 1476 (1968).
[27]R. Handler, S. C. Wright, L. Pondrom, P. Limon, S. Olsen, and P. Kloeppel, Phys. Rev. Letters 19, 933 (1967).
[28]D. Bodansky, S. F. Eccles, G. W. Farwell, M. E. Rickey, and P. C. Robison, Phys. Rev. Letters 2, 101 (1959).
[29]D. Bodansky, W. J. Braithwaite, D. C. Shreve, D. W. Storm, and W. G. Weitkamp, Phys. Rev. Letters 17, 589 (1966).
[30]W. G. Weitkamp, D. W. Storm, D. C. Shreve, W. J. Braithwaite, and D. Bodansky, Phys. Rev. 165, 1233 (1968).
[31]M. von Witsch, A. Richter, and P. von Brentano, Phys. Letters 22, 631 (1966); Phys. Rev. Letters 19, 524 (1967); Phys. Rev. 169, 923 (1968).
[32]S. Barshay, Phys. Rev. Letters 17, 49 (1966).
[33]D. I. Sober, D. G. Cassel, A. J. Sadoff, K. W. Chen, and P. A. Crean, Phys. Rev. Letters 22, 430 (1969).
[34]R. L. Anderson, R. Prepost, and B. H. Wiik, Phys. Rev. Letters 22, 651 (1969).
[35]D. F. Bartlett, C. E. Friedberg, K. Goulianos, I. S. Hammerman, and D. P. Hutchinson, Phys. Rev. Letters 23, 893, 1205(E) (1969).
[36]M. Longo, Bull. Am. Phys. Soc. 14, 598 (1969).
[37]J. K. Baird, P. D. Miller, W. B. Dress, and N. F. Ramsey, Phys. Rev. 179, 1285 (1969).
[38]G. E. Harrison, P. G. H. Sandars, and S. J. Wright, Phys. Rev. Letters 22, 1263 (1969).
[39]M. C. Weisskopf, J. P. Carrico, H. Gould, E. Lipworth, and T. S. Stein, Phys. Rev. Letters 21, 1645 (1968).
[40]D. Berley and G. Gidal, Phys. Rev. 118, 1086 (1960).
[41]J. W. Cronin and O. E. Overseth, Phys. Rev. 129, 1795 (1963); D. Bartlett, C. E. Friedberg, K. Goulianos, and D. Hutchinson, Phys. Rev. Letters 16, 282, 601(E) (1966); D. Cline, *ibid.* 16, 367 (1966); R. G. Glasser, B. Kehoe, P. Engelmann, H. Schneider, and L. E. Kirsch, *ibid.* 17, 603 (1966); R. J. Abrams, A. Abashian, R. E. Mischke, B. M. K. Nefkens, J. H. Smith, R. C. Thatcher, L. J. Verhey, and A. Wattenberg, *ibid.* 17, 606 (1966); K. K. Young, M. J. Longo, and J. A. Helland, *ibid.* 18, 806 (1967); N. Barash, T. B. Day, R. G. Glasser, B. Kehoe, R. Knop, B. Sechi-Zorn, and G. A. Snow, *ibid.* 19, 181 (1967); O. E. Overseth and R. F. Roth, *ibid.* 19, 391 (1967).
[42]S. T. Thornton, C. M. Jones, J. K. Bair, M. D. Mancusi, and H. B. Willard, Phys. Rev. Letters 21, 447 (1968).
[43]W. Heitler, *The Quantum Theory of Radiation* (Oxford University Press, London, England, 1954), 3rd ed., pp. 412–414; H. Muirhead, *The Physics of Elementary Particles* (Pergamon Press, New York, 1965).
[44]E. M. Henley and B. A. Jacobsohn, Phys. Rev. 113, 225 (1959).
[45]T. E. O. Ericson, Phys. Letters 23, 97 (1966).
[46]C. Mahaux and H. A. Weidenmüller, Phys. Letters 23, 100 (1966).
[47]T. J. Krieger, Bull. Am. Phys. Soc. 12, 498 (1967).
[48]N. Rosenzweig, Bull. Am. Phys. Soc. 12, 894 (1967).
[49]D. Robson, Phys. Letters 26B, 117 (1968).
[50]P. A. Moldauer, Phys. Rev. 165, 1136 (1968).
[51]E. M. Henley and A. H. Huffman, Phys. Rev. Letters 20, 1191 (1968).
[52]P. A. Moldauer, Phys. Letters 26B, 713 (1968).
[53]D. Pledger and H. T. Richards, private communication.
[54]C. M. Jones, J. W. Johnson, and R. M. Beckers, Nucl. Instr. Methods 68, 77 (1969).
[55]Hamilton Watch Company, Precision Metal Division, Lancaster, Pennsylvania.
[56]M. D. Mancusi, J. K. Bair, C. M. Jones, S. T. Thornton, and H. B. Willard, Nucl. Instr. Methods 68, 70 (1969).
[57]S. K. Allison, Rev. Mod. Phys. 30, 1137 (1958).
[58]W. Whaling, in *Handbuch der Physik*, edited by S. Flügge (Springer-Verlag, Berlin, Germany, 1958), Vol. 34, pp. 193–217.
[59]A. M. Thomas and J. L. Cross, J. Vac. Sci. Technol. 4, 1 (1967).
[60]*Handbook of Chemistry and Physics*, edited by C. D. Hodgman (Chemical Rubber Publishing Company, Cleveland, Ohio, 1960), 42nd ed.
[61]J. B. Marion, Rev. Mod. Phys. 38, 660 (1966).
[62]A. Rytz, H. H. Staub, H. Winkler, and F. Zamboni, Nucl. Phys. 43, 229 (1963).
[63]F. Everling, L. A. Koenig, J. H. E. Mattauch, and and A. H. Wapstra, *Nuclear Data Tables* (U. S. Government Printing Office, Washington, D.C., 1960), Pt. I.
[64]K. R. Symon, dissertation, Harvard University, 1948 [see B. R. Rossi, *High Energy Particles* (Prentice Hall, Inc., Englewood Cliffs, New Jersey, 1952)].
[65]H. R. Worthington, Ph.D. thesis, University of Wisconsin, 1952 (unpublished); H. R. Worthington, J. N. McGruer, and D. E. Findley, Phys. Rev. 90, 899 (1953).
[66]E. A. Silverstein, Nucl. Instr. Methods 4, 53 (1959).

[67]R. E. Phillips and S. T. Thornton, Oak Ridge National Laboratory Report No. ORNL-4179, 1967 (unpublished).
[68]J. Orear, University of California Radiation Laboratory Report No. UCRL-8417, 1958 (unpublished);
A. McFarlane Mood, *Introduction to the Theory of Statistics* (McGraw-Hill Book Company, New York, 1950), p. 152.

PHYSICAL REVIEW C VOLUME 3, NUMBER 3 MARCH 1971

Proton Stripping Strengths for Levels of $^{11}C^{\dagger}$

J. R. Comfort,* H. T. Fortune,‡ J. V. Maher,§ and B. Zeidman
Argonne National Laboratory, Argonne, Illinois 60439
(Received 13 November 1970)

States of ^{11}C were studied with the $^{10}B(^3He, d)^{11}C$ reaction at a bombarding energy of 21 MeV. The data were found to favor the assignments $J^{\pi} = \frac{7}{2}^+$ and $\frac{5}{2}^+$ to the levels at 8.65 and 8.69 MeV, respectively. A distorted-wave analysis of the angular distributions for negative-parity states in ^{11}C yielded spectroscopic factors whose relative values agreed well with the predictions of Cohen and Kurath, even though the excited-state energies were found to be in better agreement with the predictions of the unified rotational model.

I. INTRODUCTION

The mirror nuclei ^{11}B and ^{11}C have been extensively studied and many of their properties are known.[1] Not so well known, however, are the single-particle strengths of the states as observed in the reactions $^{10}B(d, p)^{11}B$ and $^{10}B(^3He, d)^{11}C$. These are of considerable interest, since they may be compared directly with the predictions of the nuclear shell-model calculations of Cohen and Kurath[2,3] and Goldhammer *et al.*[4,5]

In previous work, the spectroscopic strengths for (d, p) reactions,[6,7] (d, n) reactions,[8] and $(^3He, d)$ reactions[9,10] on ^{10}B have generally been derived from analyses with plane-wave Born-approximation (PWBA) stripping codes. The absolute values of the strengths thus obtained are seldom accurate, and even the relative strengths are uncertain.

It has been shown[11,12] that distorted-wave Born approximation (DWBA) analyses are reasonably capable of fitting the angular distributions for single-particle transfer reactions on targets in the $1p$ shell and that the spectroscopic factors obtained are in reasonable agreement with shell-model calculations. However, for the $^{10}B(d, p)^{11}B$ reaction, such analyses have been carried out[11] only for transitions to the three strongest states below 7-MeV excitation. Other DWBA analyses were confined to the ground-state transition.[13,14] For the $^{10}B(^3He, d)^{11}C$ reaction, a DWBA analysis has been reported[15] only for the ground-state transition at bombarding energies less than 10 MeV.

The reaction $^{10}B(^3He, d)^{11}C$ was studied here at a bombarding energy of 21 MeV. Some of these data have been discussed in a previous report[16] in which $J^{\pi} = \frac{3}{2}^-$ was assigned to the 8.11-MeV state of ^{11}C. In the present study, we consider a DWBA analysis of all states below the proton breakup threshold at 8.693 MeV. Absolute spectroscopic factors have been extracted and they are compared with the predictions of shell-model calculations.[2-5] The angular distribution of a broad ($\Gamma \approx 200$ keV) level at 10.68 MeV is presented and fitted with a distorted-wave calculation. The ground-state transition from the $^{12}C(^3He, d)^{13}N$ reaction is also discussed.

II. EXPERIMENTAL PROCEDURE

The Argonne FN tandem accelerator produced a beam of ^3He ions with an energy of about 20.9 MeV. The ^3He beam was incident on self-supporting ^{12}C and ^{10}B targets placed in the center of an 18-in. remotely controlled scattering chamber.[17] The ^{12}C target was approximately 60 $\mu g/cm^2$ thick and the ^{10}B target, enriched to about 96% ^{10}B, was about 100 $\mu g/cm^2$ thick. Each was oriented with its normal at about 30° to the beam direction. The data revealed the presence of oxygen in both targets, and traces of ^{11}B, ^{12}C, and ^{28}Si in the ^{10}B target.

A vertical beam profile on the targets was established by two beam-defining slits whose dimensions were $\frac{1}{16} \times \frac{3}{16}$ in. and which were spaced about 12 in. apart, with the second slit placed about 8 in. before the target. The solid angle subtended by the detector was also defined by a rectangular collimator of the same dimensions placed about 4 in. from the target.

The detector telescope was composed of silicon surface-barrier derectors. The ΔE detector was 500 μ thick, which was sufficient to stop the elastically scattered ^3He particles, and the E detector